DOT/FAA/AR-09/15

Air Traffic Organization
NextGen & Operations Planning
Office of Research and
Technology Development
Washington, DC 20591

Operational Usage Information for a Commuter Propeller

July 2009

Final Report

This document is available to the U.S. public through the National Technical Information Service (NTIS), Springfield, Virginia 22161.

U.S. Department of Transportation
Federal Aviation Administration

NOTICE

This document is disseminated under the sponsorship of the U.S. Department of Transportation in the interest of information exchange. The United States Government assumes no liability for the contents or use thereof. The United States Government does not endorse products or manufacturers. Trade or manufacturer's names appear herein solely because they are considered essential to the objective of this report. This document does not constitute FAA certification policy. Consult your local FAA aircraft certification office as to its use.

This report is available at the Federal Aviation Administration William J. Hughes Technical Center's Full-Text Technical Reports page: actlibrary.act.faa.gov in Adobe Acrobat portable document format (PDF).

Technical Report Documentation Page

1. Report No.	2. Government Accession No.	3. Recipient's Catalog No.
DOT/FAA/AR-09/15		

4. Title and Subtitle	5. Report Date
OPERATIONAL USAGE INFORMATION FOR A COMMUTER PROPELLER	July 2009
	6. Performing Organization Code
7. Author(s)	8. Performing Organization Report No.
Kamran Rokhsaz, Johann Dorfling, and Linda K. Kliment	
9. Performing Organization Name and Address	10. Work Unit No. (TRAIS)
Wichita State University 1840 Fairmount Wichita, KS 67260-0044	11. Contract or Grant No.
12. Sponsoring Agency Name and Address	13. Type of Report and Period Covered
U.S. Department of Transportation Federal Aviation Administration Air Traffic Organization NextGen & Operations Planning Office of Research and Technology Development Washington, DC 20591	Final Report
	14. Sponsoring Agency Code
	ANE-110

15. Supplementary Notes

The Federal Aviation Administration Airport and Aircraft Safety R&D Division technical monitor was Cu Nguyen.

16. Abstract

Wichita State University (WSU) supports the Federal Aviation Administration (FAA) research in the area of Operational Loads Measurement of commuter and general aviation aircraft. This research is aimed primarily at acquiring and reducing typical in-service usage data for the purpose of better understanding the flight loads experienced by the airframe. The program includes developing improved methods and criteria for processing and presenting large amounts of data. These activities result in information that can (1) lead to the understanding of the service-related factors affecting the operational life of the aircraft and (2) allow the FAA to reassess continued suitability of existing certification criteria.

The University of Dayton Research Institute (UDRI) published the results from the processing and analysis of digital flight recorder data obtained from 910 flights of 30 BE-1900D aircraft during typical operational usage by a single commuter airline. These aircraft employ propellers with composite structures. The data used by UDRI also contained some information on engine and propeller usage, such as engine revolutions per minute (rpm) and torque and time at propeller reversal. This report documents the efforts of WSU to derive statistical summaries of aircraft usage data, ground operations data, and flight operations data pertaining to the propellers from this database. Statistical data are presented for parameters such as torque correlated with rpm, time in propeller reversal, alpha, and unsteadiness in alpha due to gust velocities. The scope of activities performed encompasses the service-related factors that affect the operational life of the propeller, as defined by the propeller manufacturer. WSU has generated the processed data in statistical formats that can enable the FAA, the propeller manufacturer, and the airline to better understand and control those factors that influence the structural integrity of these components.

17. Key Words	18. Distribution Statement
Flight profiles, Flight loads, Ground loads, Propeller usage data	This document is available to the U.S. public through the National Technical Information Service (NTIS), Springfield, Virginia 22161.

19. Security Classif. (of this report)	20. Security Classif. (of this page)	21. No. of Pages	22. Price
Unclassified	Unclassified	70	

Form DOT F1700.7 **(8-72)** **Reproduction of completed page authorized**

PREFACE

The research reported in this document was performed by the Flight Dynamics Laboratory of the College of Engineering at Wichita State University (WSU). This effort was funded by the Federal Aviation Administration (FAA) through the Center for General Aviation Research. At WSU, the principal investigators were Dr. Kamran Rokhsaz and Ms. Linda K. Kliment of the Department of Aerospace Engineering. Mr. Johann Dorfling developed the data reduction algorithms and software and established the data reduction criteria. The format used for presentation of most of the statistical data was adopted from the work previously performed by the University of Dayton Research Institute. The contract monitor for the FAA was Mr. Cu Nguyen of the FAA William J. Hughes Technical Center, Atlantic City International Airport, New Jersey.

TABLE OF CONTENTS

		Page
EXECUTIVE SUMMARY		xi
1.	INTRODUCTION	1
2.	AIRCRAFT DESCRIPTION	2
3.	PROPELLER DESCRIPTION	3
4.	DIGITAL FLIGHT DATA RECORDER DATA AND FORMAT	4
5.	WICHITA STATE UNIVERSITY DATA PROCESSING	4
5.1	Filtering and Normalizing	4
5.2	Derived Parameters	5
5.2.1	Identification of Takeoff Rotation	5
5.2.2	Flight Distance	5
5.2.3	Flight Duration	6
5.2.4	Load Factor Definition	6
5.2.5	Derived Gust Velocity	6
5.2.6	Angle of Attack	8
5.2.7	Wing Upwash Angle	9
5.2.8	Torque and Thrust	12
5.3	Statistical Analysis	14
5.4	Available Data	16
5.5	Data Reduction Criteria	16
5.5.1	Ground Operations	17
5.5.2	Flight Operations	18
5.6	Methods of Data Extraction	20
5.6.1	Ground Operations	20
5.6.2	Operations Within Prohibited Shaft Speed Range	20
5.6.3	Flight Operations	21
5.6.4	Sign Convention	22
5.6.5	Separation of Maneuver and Gust Load Factors	23
5.6.6	Peak-Valley Selection	23
5.6.7	Altitude Bands	24
6.	DATA PRESENTATION	24

6.1 Overall Aircraft Usage 24

6.1.1 Flight Duration and Distance 24
6.1.2 Flap Usage 27
6.1.3 Overall Engine Usage 29

6.2 Ground Operations 30

6.2.1 General Ground Operations 30
6.2.2 Shaft Speed Before Shutdown 30
6.2.3 Operations Within Restricted Zone 30
6.2.4 Propeller Reversal 33
6.2.5 Takeoff Rotation 37

6.3 Flight Operations 42

6.3.1 Aerodynamics Data 42
6.3.2 In-Flight Engine and Propeller Usage 48
6.3.3 Effect of Gusts on Angle of Attack 50

7. CONCLUSIONS 54

8. REFERENCES 55

APPENDIX A—CALCULATION OF UPWASH ANGLE

LIST OF FIGURES

Figure		Page
1	Schematic of the Sources of the Inflow Angle	1
2	BE-1900D Three-View Drawing	3
3	Dimensions of the Equivalent Horseshoe Vortex Relative to the Propeller Planes	11
4	Representation of the Vibratory Stress Cycles for Each Flight	17
5	Schematic of the Flight Phases	17
6	Peak-Between-Means Classification of Loads	23
7	Number of Flights Versus Flight Duration	25
8	Percentage of Total Flight Time and Flight Distance per Flight Phase	26
9	Percentage of Total Flight Time Operating at Different Airspeeds	26
10	Percentage of Takeoffs and Landings Performed With Flaps Deployed	27
11	Beta Probability Density and Cumulative Distribution of the Airspeed at Flap Retraction—a = 120.41, b = 9.447E+7, α_1 = 3.467, α_2 = 1.108E+7	28
12	Percentage of Total Flight Time With Flaps Deployed	29
13	Percentage of Total Flight Time at Different Torque Levels	29
14	Distributed and Normal Probability Density of rpm Before Engine Shutdown μ = 1015 rpm, σ = 85.1 rpm	30
15	Percentage of Time Operating in the 400 to 950 rpm Range	31
16	Percentage of Time Operating in the 1250 to 1395 rpm Range	32
17	Time to Transition Through Restricted Propeller Shaft Speed Ranges Increasing rpm: μ = 2.067, σ = 0.890—Decreasing rpm: μ = 0.999, σ = 0.903	32
18	Indicated Airspeed at Start of Propeller Reversal	34
19	Distributed and Cumulative Lognormal Probability of Reverse Cycles Duration μ = 1.841, σ = 1.133	35

20 Distributed and Cumulative Normal Probability of rpm at Propeller Reversal Maximum: $\mu = 1107.0$, $\sigma = 123.16$—Minimum: $\mu = 984.32$, $\sigma = 119.08$ 36

21 Distributed and Cumulative Lognormal Probability of Torque at Propeller Reversal Maximum: $\mu = 6.229$, $\sigma = 0.996$—Minimum: $\mu = 5.846$, $\sigma = 1.063$ 36

22 Distributed and Cumulative Normal Probability of rpm at Takeoff Rotation $\mu = 1725.0$, $\sigma = 17.41$ 37

23 Distributed and Cumulative Normal Probability of Torque at Takeoff Rotation $\mu = 3518.0$, $\sigma = 195.98$ 38

24 Distributed and Cumulative Normal Probability of Airspeed at Takeoff Rotation $\mu = 112.11$, $\sigma = 5.029$ 38

25 Normal Probability of Angle of Attack at Liftoff, No Flap: $\mu = 4.48$, $\sigma = 0.66$—Half Flap: $\mu = 4.18$, $\sigma = 0.95$—Full Flap: $\mu = 4.00$, $\sigma = 1.12$ 39

26 Wing Upwash Angle in Ground Effect—Aircraft Weight = 17,000 lbf 40

27 Normal Probability of Inflow Angle Minus Nacelle Tilt Angle at Liftoff No Flap: $\mu = 6.02$, $\sigma = 0.66$—Half Flap: $\mu = 6.04$, $\sigma = 0.97$—Full Flap: $\mu = 5.72$, $\sigma = 1.13$ 41

28 Ground Effect on Normal Probability of the Inflow Angle at Liftoff Minus Nacelle Tilt Angle, Ground Effect: $\mu = 6.04$, $\sigma = 0.97$—No Ground Effect: $\mu = 6.58$, $\sigma = 1.04$ 42

29 Cumulative Occurrences of Angle of Attack During the Five Flight Phases 43

30 Upwash Angle as a Function of Dynamic Pressure for Various Aircraft Weights 48

31 Cumulative Occurrence $\Delta\alpha$ due to Gusts During Climb 51

32 Cumulative Occurrence $\Delta\alpha$ due to Gusts During Cruise 52

33 Cumulative Occurrence $\Delta\alpha$ due to Gusts During Descent 53

LIST OF TABLES

Table		Page
1	Number of Flights and Hours of Operations Extracted From the Data	2
2	BE-1900D Aircraft Characteristics	2
3	Recorded Flight Loads Parameters	4
4	Summary of Distributions Used for Presentation of Aircraft Operations Data	15
5	Summary of Criteria Used for the Identification of the Ground Phases	18
6	Summary of Criteria Used in the Identification of the Five Flight Phases	19
7	BE-1900D Flap Detents	22
8	Peak-Valley Deadband Limits	23
9	Altitude Bands Above Airports	24
10	Use of Reverse Thrust After Landing	33
11	Percentage of Occurrence of Angle of Attack and Coincident Dynamic Pressure	45
12	Correlation of Engine Torque and Propeller Shaft Speed as a Percentage of Flight Time	49
13	Correlation of Thrust and Propeller Shaft Speed as a Percentage of Flight Time	49

LIST OF SYMBOLS AND ACRONYMS

C_{l_α}	Wing lift-curve slope per radian
C_T	Thrust coefficient
K_g	Discrete gust alleviation factor, $0.88\ \mu/(5.3 + \mu)$
t	Time (sec)
T	Thrust (pound)
ϕ	Pitch angle
σ	Variance
$\Delta\psi$	Change in peaks and valleys
$\Delta\sigma$	Change in angle of attack
1P	Once-per-revolution
A-D	Anderson-Darling
CFR	Code of Federal Regulations
DFDR	Digital flight data recorder
FAA	Federal Aviation Administration
fpm	Feet per minute
GAG	Ground-air-ground
IAS	Indicated airspeed
KIAS	Knots indicated airspeed
rpm	Revolutions per minute
UDRI	University of Dayton Research Institute
WSU	Wichita State University

EXECUTIVE SUMMARY

The Federal Aviation Administration Airport and Aircraft Safety Research and Development Division funded Wichita State University to conduct a survey of the operational environment of the propellers on a fleet of commuter aircraft. The program involved analyzing and extracting data from actual operational flight and ground loads data collected from digital flight data recorders installed on a fleet of aircraft operated by a single commuter airline. This collected data was of special interest because these propellers were constructed of foam core, covered with Kevlar®, and attached to an aluminum shank.

The material for this analysis consisted of data collected from 910 flight operations recorded on a fleet of 30 BE-1900D Beechcraft during routine commuter service. Basic flight parameters such as airspeed, altitude, flight duration, bank and pitch angles, and flap usage were recorded. Included in the data were some propulsion-related information and vertical load factors. Additional parameters, such as vertical speed, angle of attack, and vertical gust speeds, were not recorded but inferred from the recorded data.

In this report, statistical usage data are provided on the following:

- Torque versus revolutions per minute (rpm) in flight (to understand if high torque is being applied at low rpm)
- Probability of flap retraction versus airspeed (to understand when and how slow flap retraction occurs)
- Probability of time versus airspeed when in flight (to understand the percentage of time spent in climb versus cruise)
- Probability of time versus torque when in flight (to understand the percentage of time at high torque)
- Alpha derived from flight parameters versus coincident dynamic pressure
- Cumulative occurrences of derived gust velocities
- Cumulative occurrences of variations in alpha due to turbulence
- Probability of minimum rpm during reverse and before shutdown (to understand ground operations)
- Probability of a particular rpm during reverse and before shutdown (to understand ground operations)
- Accumulated time spent operating within the ground restrictions
- Typical time per transitioning through the ground restrictions
- “g” loading versus airspeed (to help understand the significance of gusts)

The statistical formats used here allowed an objective comparison of the existing certification and design criteria to actual usage data, thereby affording the aircraft manufacturer and operators a better understanding and control of those factors that influence the structural integrity of commuter aircraft. This data could also be used by both original equipment manufacturers and designated engineering representatives for repair and/or alterations.

1. INTRODUCTION.

Propeller blade separation is the leading contributor to accidents and serious incidents caused by a propeller on both general aviation and transport airplanes [1]. Damage tolerance of the propeller structure provides a means to reduce the incident rate for blade separation. The application of damage tolerance methods requires the establishment of propeller loads spectra.

The effectiveness of the damage tolerance analysis depends on several factors that include accurate propeller usage information. A Notice of Proposed Rulemaking was published in the Federal Register on April 11, 2007, proposing revision of Title 14 Code of Federal Regulations (CFR) 25.907 and 23.907 to require failure due to fatigue to be avoided throughout the operational life of the propeller using the data provided by 14 CFR 35.37 [2-6].

One of the largest contributors to the vibratory aerodynamic loads on the propeller is the angle of inflow into the propeller disk. This angle is a combination of the angle of attack, the engine nacelle tilt angle, and the upwash created by the wing. These quantities are shown schematically in figure 1. As a result of the angular inflow into the propeller plane, a downward moving blade experiences a greater angle of attack than an upward moving blade. This creates a difference in the thrust produced by the blade that varies in an almost sinusoidal manner as the blade turns. Furthermore, one side of the disk generates more thrust, leading to a yawing moment (P factor).

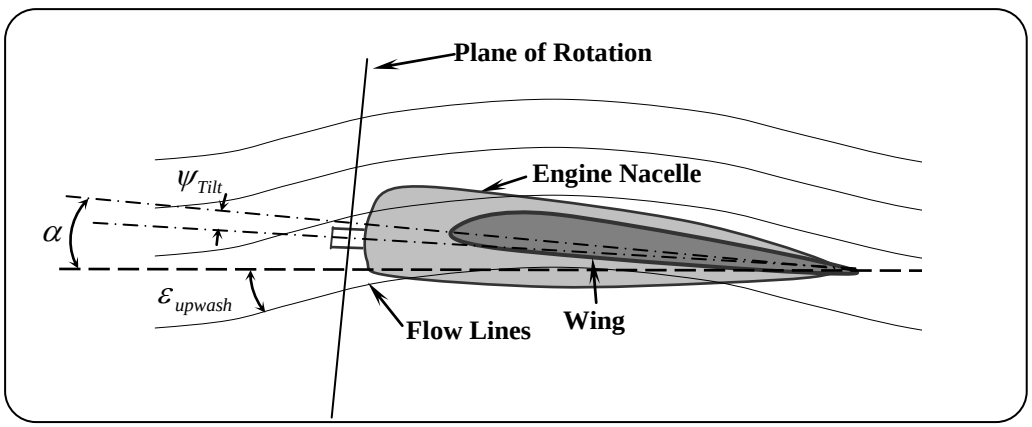

Figure 1. Schematic of the Sources of the Inflow Angle

Propellers have been almost exclusively designed and certified using the safe-life approach for their predicted operational usage. The objective of this program was to compile the in-service usage information, in statistical form, for a propeller of composite structure employed on a fleet of BE-1900D Beechcraft aircraft. The data was extracted from in-service information recorded by digital flight data recorders (DFDR) on these aircraft.

Operational data was collected from DFDRs installed on a fleet of 30 BE-1900D commuter aircraft. Wichita State University (WSU) received the data via University of Dayton Research Institute (UDRI), which had previously used it to analyze the operational flight loads on these aircraft. Data from three aircraft had to be omitted due to a variety of recording errors. Therefore, the data consisted of 910 flight files from 27 aircraft. Table 1 shows the number of flight files for each aircraft, along with the number of hours of ground and flight operations.

Table 1. Number of Flights and Hours of Operations Extracted From the Data

Aircraft No.	Number of Flights	Flight Hours	Ground Hours	Aircraft No.	Number of Flights	Flight Hours	Ground Hours
1	30	23.2	7.9	15	29	22.0	8.5
2	44	23.0	6.7	16	41	20.7	7.8
3	27	20.9	9.2	17	34	18.8	7.5
4	32	23.5	6.8	18	28	25.5	6.6
5	34	20.3	7.5	19	33	22.9	6.9
6	22	14.8	6.2	20	25	24.4	6.0
7	34	21.9	7.6	21	34	23.3	7.7
8	34	20.9	7.3	22	30	17.8	6.8
9	34	21.8	7.7	23	23	22.4	9.7
10	42	23.7	7.2	24	34	19.4	8.0
11	33	22.2	6.9	25	44	20.0	8.3
12	38	22.8	9.2	26	39	25.3	7.4
13	41	22.2	8.1	27	33	23.0	8.2
14	38	22.5	8.8	Total	910	589.1	206.5

This report includes some aircraft usage and statistical data derived from recorded data to gain a better understanding of the operational environment of the propellers on these aircraft. Basic statistical information on a variety of parameters is shown in formats that can be easily compared to the manufacturer's existing design criteria. This information includes variations in aircraft angle of attack affecting the propeller inflow angle, estimates of the upwash angle in various flight phases, and statistical usage of the propeller during flight and ground operations.

2. AIRCRAFT DESCRIPTION.

Some of the operational characteristics of the BE-1900D aircraft equipped with DFDR are shown in table 2. The three-view drawing of the aircraft is shown in figure 2. (The information in table 2 and figure 2 were reproduced from reference 7.)

Table 2. BE-1900D Aircraft Characteristics

Parameter	Value
Maximum taxi weight	17,060 lb
Maximum takeoff weight	16,950 lb
Maximum landing weight	16,600 lb
Zero-fuel weight	15,000 lb
Operating empty weight*	10,350 lb*
Fuel capacity	668 U.S. gallons
Two P&W PT6A-76D turboprops	1,279 sharp horsepower each

Table 2. BE-1900D Aircraft Characteristics (Continued)

Parameter	Value
Wing span	57 ft 11.25 in.
Wing reference area	310 ft^2
Wing Mean Aerodynamic Chord	5.32 ft
Length	57 ft 10 in.
Height	15 ft 6 in.
Tread	17 ft 2 in.
Wheel base	23 ft 9.5 in.

*Note: Operating Empty Weight is not a [1] value but was provided by the airline [7]
P&W = Pratt & Whitney

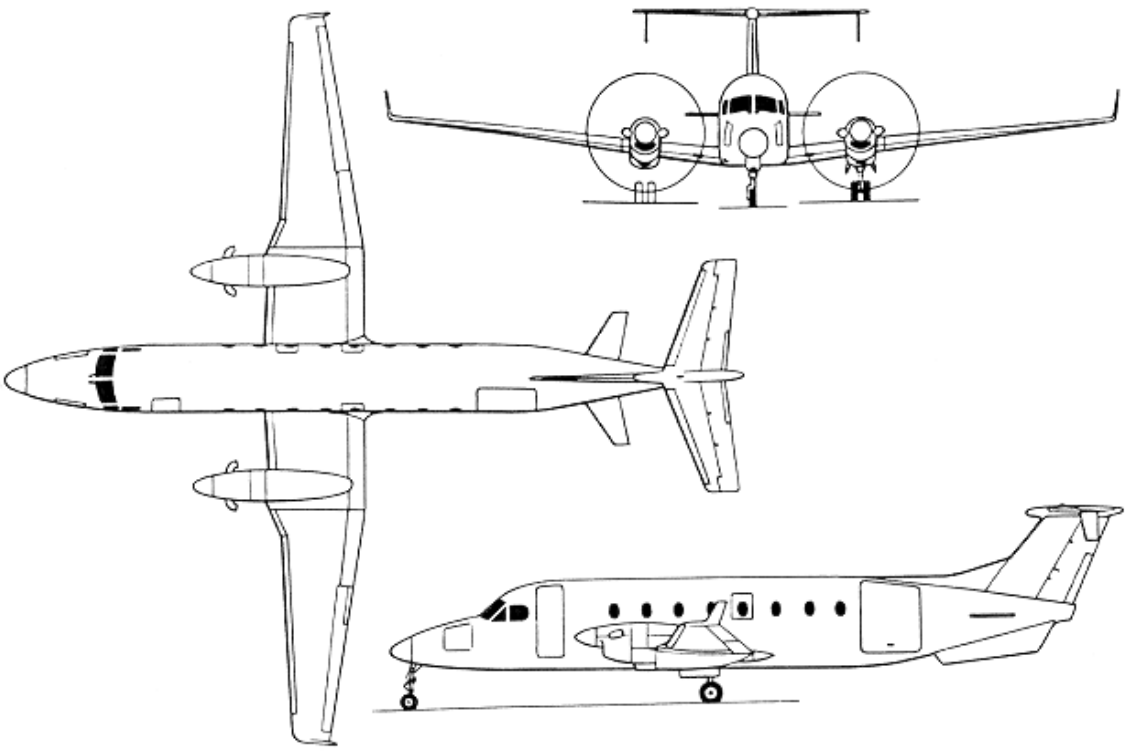

Figure 2. BE-1900D Three-View Drawing [7]

3. PROPELLER DESCRIPTION.

The aircraft are fitted with two, four-bladed Hartzell Propeller, Inc. aramid composite, 110-inch-diameter propellers [8]. The propeller is constructed of a polyurethene foam core covered with a laminated Kevlar shell. Two unidirectional Kevlar spars run along the leading and trailing edges of the blade. The blade attaches to an aluminum shank at its root. The shank is then inserted into an aluminum hub assembly. The leading edge of the blade is covered with a metal strip for erosion prevention [9 and 10].

4. DIGITAL FLIGHT DATA RECORDER DATA AND FORMAT.

The aircraft in this study were fitted with a Fairchild F1000 DFDR. A recording device developed by Systems and Electronics, Inc. was added to the aircraft to allow the information gathered by the DFDR to be stored over a much longer time period for post processing. Raw flight data was extracted and converted into DOS file formats by the airline ground editing station and copied onto hard disks. This editing station also performed an integrity check of the flight data and removed flight-sensitive information [7]. The data was received in text file format. The parameters recorded by the DFDR are summarized in table 3.

Table 3. Recorded Flight Loads Parameters

Parameter (Units)	Sample Rate	Units
Vertical acceleration	8 Hz	g
Longitudinal acceleration	4 Hz	g
Pitch angle	4 Hz	degree
Bank angle	2 Hz	degree
Pitch control	2 Hz	degree
Pressure altitude	1 Hz	ft
Indicated airspeed	1 Hz	KIAS
Magnetic heading	1 Hz	degree
rpm (left and right)	1 Hz	rpm
Engine torque (left and right)	1 Hz	ft-lbf
Prop reverse (left and right)	1 Hz	discrete
Flap position	1 Hz	discrete

rpm = Revolutions per minute
KIAS = Knots indicated airspeed

5. WICHITA STATE UNIVERSITY DATA PROCESSING.

5.1 FILTERING AND NORMALIZING.

The resolution in the recorded altitude made it impossible to calculate a reliable rate of climb. The rate of climb parameter was needed for separating flight phases and for determining the flight path angle. Therefore, the recorded altitude was filtered, using a 10-second running average.

The data during the first 20 seconds of each file was ignored to alleviate the effects of system start-up transients. All accelerometer output values were normalized relative to the 20-second average of their data while the aircraft was on the ground prior to the flight. This meant using the average acceleration output for t = 21 to 40 seconds.

5.2 DERIVED PARAMETERS.

Some information, such as rate of climb, was not recorded, and therefore, had to be extracted or derived from the time history of other parameters. In those cases when aircraft parameters had to be derived (e.g., aircraft lift-curve slope), for consistency, the values were obtained from reference 7. In addition, since the recorded data contained no information about the aircraft inertial properties, a weight of 16,500 pounds was used when needed. Issues pertaining to specific calculations and the derivations of the required parameters are described in the following sections.

5.2.1 Identification of Takeoff Rotation.

The pitch attitude was averaged over the takeoff roll, and a change of more than 2 degrees from the average value was labeled as the point of takeoff rotation. This was not necessarily the point of liftoff, but rather, the point where the rotation for takeoff was initiated. In the few seconds following this rotation, the maximum angle of attack and the greatest inflow angle into the propeller disk would be reached. Accordingly, the point of maximum angle of attack within the 10 seconds after the takeoff rotation was called the point of liftoff. This point was of interest because the aircraft might have been a few feet above the ground at the liftoff point. This point would coincide with the maximum inflow angle, although this large inflow angle would lead to the highest once-per-revolution (1P) loads on the propeller blades.

5.2.2 Flight Distance.

Flight distance was calculated by integrating the true airspeed. Previous work in this area showed the error due to wind speed to be very small.

Flight distance from integration of the true airspeed was determined from

$$D = \sum_{t_{liftoff}}^{t_{touchdown}} V_T(\Delta t) \tag{1}$$

where:

D	=	distance
V_T	=	true airspeed
Δt	=	time increment

Again, in the absence of additional information, the indicated airspeed was assumed to be the same as the calibrated airspeed. Also, since the airspeeds were not large enough to require inclusion of compressibility effects, true airspeed was derived from the indicated airspeed using the ratio of air densities, that is

$$V_T = V_C\sqrt{\frac{\rho_0}{\rho}} \approx V_i\sqrt{\frac{\rho_0}{\rho}} \tag{2}$$

where:

V_C = calibrated airspeed
V_i = indicated airspeed
ρ_0 = sea level air density
ρ = local air density

In the absence of pressure and temperature recordings, local air density was derived from the pressure altitude, assuming standard atmosphere. Therefore, local density was derived from

$$\rho = \rho_0 \left(1 - 6.876 \times 10^{-6} \times H_p\right)^{4.256} \tag{3}$$

where:

ρ_0 = 0.0023769 slug/ft^3 is air density at sea level
H_p = pressure altitude (ft)

5.2.3 Flight Duration.

The flight duration is defined as the time from aircraft liftoff to touchdown.

5.2.4 Load Factor Definition.

Load factors were divided into maneuver and gust based on their durations in accordance with reference 8. Load factors lasting two seconds or longer were considered due to maneuvers, while the rest were placed in the category of gust.

5.2.5 Derived Gust Velocity.

Derived gust velocities were calculated from measured normal accelerations, only for vertical gusts. For these calculations, air density was estimated from equation 3. Equivalent airspeed was determined from

$$V_e = V_T \sqrt{\frac{\rho}{\rho_0}} \tag{4}$$

where:

V_e = equivalent airspeed (ft/s)

Earlier, it was explained that for lack of additional information, calibrated airspeed was assumed to be the same as indicated airspeed. This led to the equality of the equivalent airspeed and indicated airspeed.

With this information, derived gust velocity was computed from the values of gust incremental normal acceleration as

$$U_{de} = \frac{\Delta n_z}{\overline{C}} \tag{5}$$

where:

U_{de} = derived gust velocity (ft/s)
Δn_z = incremental vertical load factor (g)

The aircraft response factor, $\overline{C}$, was calculated from

$$\overline{C} = \frac{\rho_0 V_e C_{L_\alpha} S}{2W} K_g \tag{6}$$

where:

ρ_0 = 0.002377 slug/ft^3, standard sea level air density
V_e = equivalent airspeed (ft/s)
C_{L_α} = aircraft lift-curve slope (per radian)
S = wing reference area (ft^2)
W = 16,500 lb, gross weight
K_g = $\frac{0.88\mu}{5.3+\mu}$, gust alleviation factor
μ = $\frac{2W}{\rho g \overline{c} C_{L_\alpha} S}$, reduced mass
ρ = air density at altitude from equation 3
g = 32.17 ft/s^2, acceleration of gravity
$\overline{c}$ = wing mean geometric chord (ft)

Following the procedure used in reference 1, aircraft lift-curve slope, C_{L_α}, was determined from wing lift-curve slope, C_{l_α}, given by

$$C_{l_\alpha} = \frac{2\pi A_r}{2 + \left[4 + A_r^2 \beta^2 \left(1 + \frac{\tan^2 \Lambda}{\beta^2}\right)\right]^{1/2}} \tag{7}$$

where:

A_r = b^2 / S, wing aspect ratio
b = wing span (ft)
β = $\sqrt{1-M^2}$, compressibility effect
C_{l_α} = wing lift-curve slope (per radian)
Λ = wing quarter-chord sweep angle
M = V_T / a, flight Mach number
a = $a_0\sqrt{\left(1-6.876\times10^{-6}H_p\right)}$, local speed of sound (ft/s)
a_0 = 1,116.4 ft/s, speed of sound at sea level

The derived gust velocity affected instantaneous changes in angle of attack, $\Delta\alpha$, that were estimated using equation 8.

$$\Delta\alpha = \tan^{-1}\left(\frac{U_{de}}{V_T}\right) \tag{8}$$

5.2.6 Angle of Attack.

The angle of attack was estimated from a flight dynamics approach and extracted from the difference between the pitch attitude and the flight path angle. The zero lift line of the aircraft was assumed to be coincident with a zero-degree pitch attitude. However, due to inconsistencies among the data files of the recorded pitch attitude while on the ground, the zero-degree pitch attitude was set equal to the average attitude during the takeoff roll. Accordingly, all in-flight pitch angles used in the estimation of the angle of attack were referenced to the takeoff roll average. This resulted in the takeoff roll angle of attack also being equal to zero degrees since there was no flight path angle on the ground. Flight path angle was calculated from the vertical speed and true airspeed of the airplane. Vertical speed, however, was not a recorded parameter and had to be extracted from the time history of filtered pressure altitude data.

Since the pressure altitude was recorded at 1 Hz, the vertical speed was simply the difference between every two consecutive filtered values. The flight path angle, γ, was then found using equation 9.

$$\gamma = \sin^{-1}\left(\frac{V_V}{V_T}\right) \tag{9}$$

where:

γ = climb angle (deg)
V_V = vertical speed (ft/s)

To account for the pitch attitude being recorded at 4 Hz, the average value of this parameter for each second was used in the calculation of the angle of attack. The angle of attack, α, is given in equation 10.

$$\alpha = \theta - \gamma \tag{10}$$

where:

α = angle of attack (deg)

In the absence of information on the aircraft's weight and lift coefficient data, this approximation of the angle of attack had to be used. This method is limited to rectilinear flight with the wings level as turning flight would tend to increase the aircraft's g-loading and, accordingly, the angle of attack. Therefore, the angle of attack was computed only for bank angles less than 5 degrees.

The cumulative occurrences of the angle of attack per 1000 hours and per nautical mile during each of the five flight phases were then determined.

5.2.7 Wing Upwash Angle.

The inflow angle is a combination of the angle of attack, the engine nacelle tilt angle, and the upwash created by the wing. The method used for determining the angle of attack of the aircraft was discussed in section 5.2.6. The nacelle tilt angle is a geometric property of the airplane and does not require further discussion other than noting that this detailed geometric information of the BE-1900D was not available. The wing upwash angle could be determined in a variety of ways with varying degrees of complexity. Within the scope of the current project, this quantity was estimated using the equivalent horseshoe vortex method.

5.2.7.1 Equivalent Horseshoe Vortex Method.

In this method, the nonuniformly distributed lift along the span is assumed to be generated by a single vortex filament placed at the quarter chord of the wing. The strength of the equivalent horseshoe vortex, Γ_e, is proportional to the weight of the aircraft, which is equal to the lift in nonmaneuvering flight, as shown in equation 11.

$$L = W = \rho V_T \Gamma_e b_e \tag{11}$$

where:

L	=	total lift (lb)
W	=	aircraft weight (lb)
ρ	=	local air density (slug/ft^3)
Γ_e	=	equivalent horseshoe vortex strength (ft^2/s)
b_e	=	equivalent wing span (ft)

The equivalent wing span is somewhat smaller than the actual span and is a function of how lift is distributed along the span. Assuming this distribution is elliptic, the equivalent and the actual spans are related through equation 12.

$$b_e = \frac{\pi}{4} b \tag{12}$$

where:

b	=	actual wing span (ft)

The basic assumptions behind this method are that the equivalent horseshoe vortex generates the same total circulation as the wing, and the total vortex strength in the wake remains the same as that behind the actual wing. The combination of these allow for determining the equivalent vortex strength and the equivalent span simultaneously, given the characteristics of the actual wing. Once these quantities are determined, the Biot-Savart law can be used to estimate the velocities induced by the wing in its vicinity. The details of the Biot-Savart law are given in appendix A.

5.2.7.2 Estimation of the Upwash Angle.

Using the equations shown in appendix A, the upwash velocity generated by the wing at the plane of the propeller was estimated from the aircraft weight and the wing geometry. During takeoff rotation, ground effect was also included using the image method, while it was neglected in other phases of flight.

Detailed dimensions of the BE-1900D, such as the positions of the engine nacelles and the locations of the propeller plane, were not available. Therefore, these dimensions were estimated from the schematic of the aircraft shown in figure 1. The locations of the propeller plane relative to the bound vortex located at the quarter chord of the wing and the trailing vortices were needed in the calculation of the upwash velocity. Figure 3 shows the top view of the aircraft with the dimensions used for the subsequent analysis. As indicated in this figure, the upwash was determined at the center of the plane of the propeller (i.e., the base of the spinner).

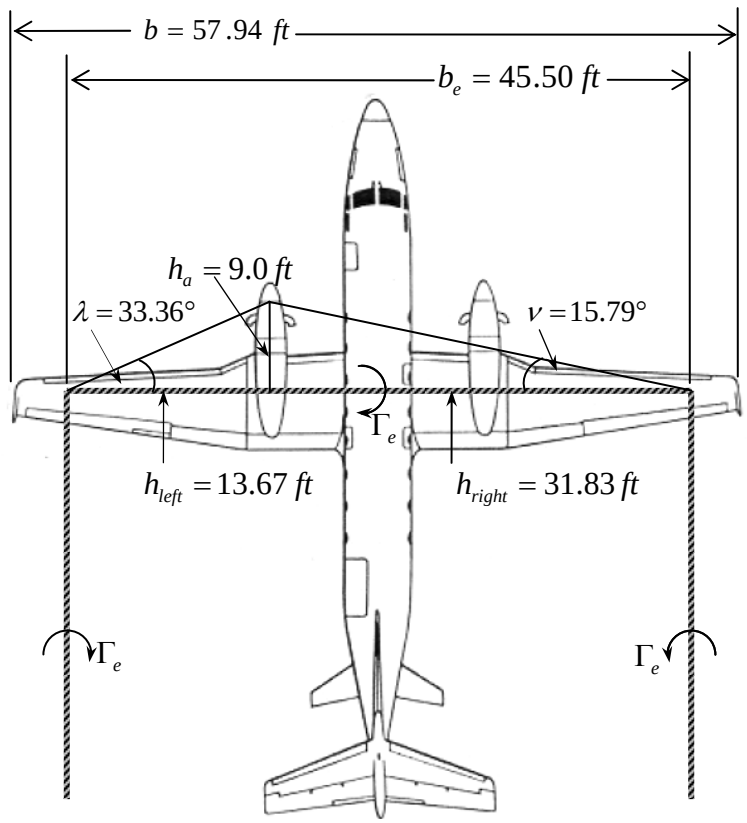

Figure 3. Dimensions of the Equivalent Horseshoe Vortex Relative to the Propeller Planes

Three filaments constituted the equivalent horseshoe vortex system: two semi-infinite trailing vortices and one bound vortex, all of strength Γ_e. Each vortex contributed to the total upwash velocity. The two trailing vortices induced a downward velocity at the plane of the propeller while the bound vortex induced an upward velocity. The total velocity induced at the plane of the propeller was the sum of the three induced flow velocity vectors. Due to symmetry, the induced velocities were equal in the planes of both propellers.

Adding the contributions of the three vortex filaments resulted in the upwash velocity given by equation 13.

$$v = \frac{W}{4\pi\rho\, V_T b_e}\left\{\frac{1}{h_a}\left(\cos\lambda + \cos\nu\right) - \frac{1}{h_{left}}\left(1 - \sin\lambda\right) - \frac{1}{h_{right}}\left(1 - \sin\nu\right)\right\} \tag{13}$$

where:

v	=	upwash velocity at the plane of the propeller (ft/s)
W	=	aircraft weight (lb)
ρ	=	local air density (slug/ft^3)

V_T = true airspeed (ft/s)
b_e = equivalent wing span (ft)
h_a = shortest distance from the bound vortex to the plane of the propeller (ft)
h_{left} = shortest distance from the left trailing vortex to the plane of the propeller (ft)
h_{right} = shortest distance from the right trailing vortex to the plane of the propeller (ft)

After determining the upwash velocity at the plane of the propeller, the upwash angle, ε, was found from equation 14.

$$\tan(\varepsilon) = \frac{v}{V_T} \tag{14}$$

5.2.7.3 Special Considerations for Ground Effect.

When an aircraft is operated within ground effect, the curvature of the streamlines ahead of the wing is reduced. Thus, the amount of upwash produced by a wing within ground effect is less than an equivalent wing flying outside ground effect at the same weight and dynamic pressure.

Ground effect was estimated using the image method, which was done by placing a mirror horseshoe vortex system underground. This vortex system was the mirror image of the equivalent horseshoe vortex on the aircraft. The ground acted as a plane of symmetry between the two vortex systems. The Biot-Savart law was used again in the same fashion as discussed in section 5.2.7.2, except in this case, different lengths and angles from those shown in figure 3 had to be used. The lengths and angles were dependent on the height of the propeller axis above the ground.

The net effect of the underground vortex system was a downward-induced flow velocity, and thus, the total upwash velocity in ground effect was then given by equation 15.

$$v_{tot} = v_{upwash} - v_{GE} \tag{15}$$

The effect of the underground vortex system became negligible at an altitude above ground level roughly equivalent to the wingspan of the aircraft. Therefore, ground effect was not included in the calculations beyond takeoff rotation.

5.2.8 Torque and Thrust.

Performance maps provided by Hartzell Propeller, Inc. were used to find the thrust versus propeller shaft speed while in flight. Since outside air temperature was not a recorded parameter, standard atmospheric conditions were assumed. Local air density and true airspeed were estimated from equations 2 and 3. The thrust generated by the propellers had to be extracted from these maps using the shaft speed, torque, true airspeed, and pressure altitude. Maps were provided for various propeller tip Mach numbers. The thrust coefficient was related to power coefficient and advance ratio in the propeller maps. These quantities are defined in the following equations.

$$J = \frac{V_T}{nD} \tag{16}$$

$$C_p = \frac{P}{\rho n^3 D^5} \tag{17}$$

$$M_{tip} = M_\infty \sqrt{1 + \left(\frac{\pi}{J}\right)^2} \tag{18}$$

where:

J	=	advance ratio
V_T	=	true airspeed (ft/s)
n	=	shaft speed (rev/s)
D	=	propeller disk diameter (ft)
C_P	=	power coefficient
P	=	power (ft-lbf/s)
ρ	=	local air density (slug/ft^3)
M_{tip}	=	propeller blade tip Mach number
M_∞	=	flight Mach number

Power was determined from the product of the torque and the propeller shaft speed. The propeller tip Mach number was a function of the free-stream Mach number and the advance ratio. The free-stream Mach number was determined from the ratio of the aircraft true airspeed to the local speed of sound, which was found from

$$a = a_0 \sqrt{\left(1 - 6.876 \cdot 10^{-6} \cdot H_p\right)} \tag{19}$$

where:

a	=	local speed of sound (ft/s)
a_0	=	speed of sound at sea level (ft/s)
H_p	=	local pressure altitude (ft)

Knowing the above, the thrust coefficient was extracted from the propeller maps. This parameter is defined as

$$C_T = \frac{T}{\rho_\infty n^3 D^4} \tag{20}$$

The propeller shaft speed was again divided into 20 bands between 800 and 1800 revolutions per minute (rpm), and the thrust separated into 17 bands of equal width between 0 and 3400 lbf, and one band that included all thrusts greater than 3400 lbf. Similar to the torque versus shaft speed data, the number of occurrences of thrust and shaft speed combinations were obtained and converted to percentages of the total flight time.

5.3 STATISTICAL ANALYSIS.

One of the goals of this project was to describe the information contained in the large amount of flight data in statistical form to assist the operators, the regulators, and the manufacturers gain a better understanding of the actual propeller usage. For some of the parameters considered in this study, representation with the standard normal distribution was not appropriate. For example, a normal distribution would have suggested a negative value of a parameter, such as time or torque, to be probable when in fact it was physically impossible. To aid in the selection of an appropriate statistical distribution in such cases, the Anderson-Darling (A-D) goodness-of-fit test was used. This goodness-of-fit test, which is very similar to the Kolmogorov-Smirnov (K-S) test, is a method of determining how well a hypothesized distribution fits the data set. However, the A-D test detects discrepancies in the low-probability regions, which is where many distributions differ [11].

The data for airspeed at the start of a reverse cycle produced a double-hump distribution. Applying a simple distribution to this data would have resulted in the loss of this unique trend. In cases like this, the investigators' judgment determined the appropriate distribution to describe the data. For this particular case, a bar chart was determined to be a more appropriate representation than a statistical distribution to ensure the preservation of the double hump.

Another reason for not using a normal distribution for some parameters was because the A-D goodness-of-fit test indicated that another distribution was more suitable for the data, e.g., the airspeed at flap retraction where a beta distribution was used. For both the flight and ground operations data, the A-D goodness-of-fit test often suggested the use of distributions different from those used. The investigator's judgment prevailed in such cases. The most important attribute of a distribution was reasoned to be an accurate portrayal of the trends observed in the data. However, rather than using obscure distributions that the A-D test showed to be slightly better, it was decided to use the better known distributions. This ensured the results of this study could be used without the need for an extensive knowledge of statistics. Table 4 shows the parameters that required statistical representation, along with the distributions and statistical parameters used to describe each.

Table 4. Summary of Distributions Used for Presentation of Aircraft Operations Data

Parameter	Distribution	Statistics
Flap retraction airspeed	Beta	α = 120.41, b = 9.447E+7
		α_1 = 3.467, α_2 = 1.108E+7
rpm before shutdown	Normal	μ = 1015.3
		σ = 85.122
Restricted rpm transition (increasing)	Lognormal	μ = 2.067
		σ = 0.890
Restricted rpm transition (decreasing)	Lognormal	μ = 0.999
		σ = 0.903
Time in reverse	Lognormal	μ = 1.841
		σ = 1.133
Maximum rpm during reverse	Normal	μ = 1107.0
		σ = 123.16
Minimum rpm during reverse	Normal	μ = 984.32
		σ = 119.08
Maximum torque during reverse	Lognormal	μ = 6.229
		σ = 0.996
Minimum torque during reverse	Lognormal	μ = 5.846
		σ = 1.063
rpm at rotation	Normal	μ = 1725.0
		σ = 17.41
Torque at rotation	Normal	μ = 3518.0
		σ = 195.98
Airspeed at rotation	Normal	μ = 112.11
		σ = 5.029
Liftoff angle of attack (no flaps)	Normal	μ = 4.477
		σ = 0.655
Liftoff angle of attack (approach flaps)	Normal	μ = 4.1835
		σ = 0.946
Liftoff angle of attack (full flaps)	Normal	μ = 4.000
		σ = 1.121
Liftoff inflow angle (no flaps)	Normal	μ = 6.019
		σ = 0.657
Liftoff inflow angle (approach flaps)	Normal	μ = 6.039
		σ = 0.972
Liftoff inflow angle (full flaps)	Normal	μ = 5.724
		σ = 1.129
No ground effect (approach flaps)	Normal	μ = 6.579
		σ = 1.040

5.4 AVAILABLE DATA.

Flight data from 30 BE-1900D aircraft was received in text file format—one file for each aircraft and each file contained data from multiple flights. Of the 30 files, 3 files were completely excluded from the study as some of the recorded parameters in these files were plagued by errors. Although the remaining 27 files contained some errors, these errors were typically not present throughout the entire file; thus, only the affected parts of the files had to be excluded from the analysis.

An inverted reverse propeller parameter was a common error found in the data files. If a data file contained this error, it persisted throughout the entire file. When this error was present, the parameter indicated a reversal throughout an entire flight. Furthermore, when the propeller was actually put in reverse, the data indicated that it was out of reverse. This was obviously opposite to what actually occurred and thus easily recognizable. Files affected by this error could easily be corrected by simply inverting the reverse propeller parameter, resulting in the inclusion of these files in the investigation.

Some of the data files were plagued by a nonsequential timing error. Typically, four lines of data would be in sequence, followed by another four lines that would be in sequence with each other, but not with the preceding four lines. This timing error was generally only present for the first few thousand lines of data, but it also occurred in random locations in a few files. Since this error did not affect the data files in their entirety, the affected flights in the files were excluded from the analysis, resulting in the majority of the data from these files being used.

Two of the three files excluded from the study had incorrectly recorded values of engine torque. This error was identified by comparing the torque values in these two files to those in other files. The third file was excluded because its flap position, parameter was inoperative. The flaps were always recorded as being in the up position, except for a second or two at random locations in the file. The affected parameters in these files were important to this study, and thus could not be included in the analysis.

Overall, the quality of the data was very good, and the majority of the data was used in the investigation. Very few errors were present in the 27 files, resulting in the extraction of flight data for 910 flights, representing about 589 flight hours.

5.5 DATA REDUCTION CRITERIA.

Figure 4 shows a schematic of the loading history of a propeller during a ground-air-ground (GAG) cycle. It is evident that in each cycle, an aircraft goes through distinctly different phases of flight, and each segment produces unique loading conditions on the propeller. Accordingly, flights were separated into a number of different phases identified as either a major portion of each flight or one of special interest in terms of propeller loading. The data was divided into two main categories: ground operations and flight operations. These two broad categories were further subdivided into various smaller phases. Figure 5 shows a schematic of the flight phases used for the subsequent analysis. The methods used for separating each of these phases, as well some of the parameters of interest during each phase, are discussed in the following sections.

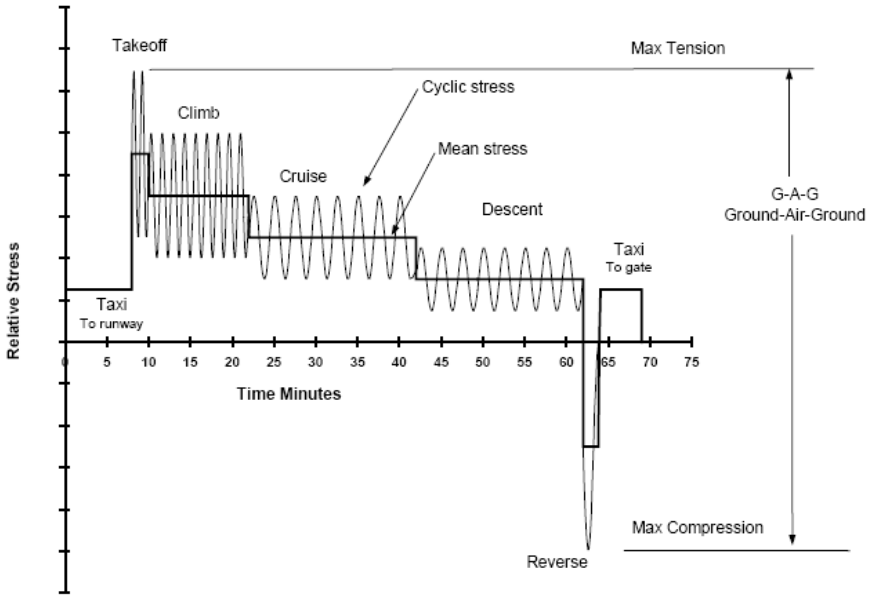

Figure 4. Representation of the Vibratory Stress Cycles for Each Flight

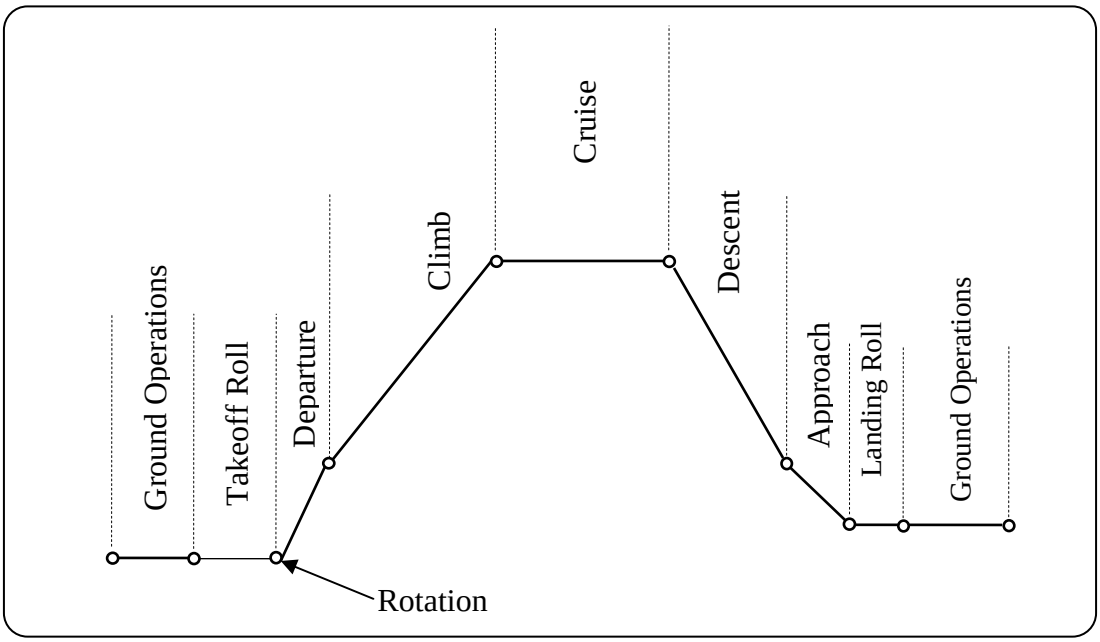

Figure 5. Schematic of the Flight Phases

5.5.1 Ground Operations.

The ground operations were subdivided into three categories: (1) general ground operations, (2) ground operations involving propeller reversal, and (3) the takeoff roll. In the absence of a weight-on-wheel recording (i.e., squat switch position), a landing configuration stalling speed of 84 knots, indicated in reference 13, was used for identification. Therefore, the only criterion necessary for the identification of general ground operations was an indicated airspeed of less

than 84 knots. One of the issues of interest here was the stabilized operation within the restricted propeller shaft speed ranges of 400 to 950 rpm and 1250 to 1395 rpm. The reason for these restrictions was not clear, but could possibly be to prevent the excitation of resonance frequencies in the propeller, engine, or airframe. Other issues considered during general ground operations were the time to transition through the restricted shaft speed bands as well as the stabilized shaft speed before engine shutdown.

The next ground operation was the reverse cycle. The primary purpose of reverse thrust is to aid in the braking of the airplane during a landing rollout, but this function is also used for braking while taxiing and maneuvering on the ground. Since reverse cycles occur during the landing rollout where the airspeed might be greater than 84 knots (i.e., immediately after touchdown), this event could not be considered part of the general ground operations. Selection of reverse thrust while in flight was considered to be a very unlikely event as the propeller governors on the BE-1900D employ flight idle stops [14]. Due to these factors, the identification of this phase only required the use of the reverse propeller parameter. The parameters of interest during propeller reversals were the airspeed, propeller shaft speed, and engine torque at which this event occurred, as well as the duration of this event.

The final ground operation, the takeoff roll, was identified using the indicated airspeed (IAS). For the majority of ground operations, the indicated airspeed was recorded in the data files as less than 50 knots. The airspeed exceeded 50 knots during flight, landing rollout, or takeoff roll only. Therefore, the point where the airspeed exceeded 50 knots with an increasing trend was called the start of the takeoff roll. The end of the takeoff roll occurred either at liftoff or upon a decrease in airspeed. The point of interest during the takeoff roll was the takeoff rotation since this was identified as one of the most critical phases of flight in terms of cyclic loading on the propeller disk. Figure 4 shows the typical loading a propeller experiences during a GAG cycle. As shown in this figure, the greatest blade stress during a GAG cycle occurs during takeoff rotation. The parameters studied at takeoff rotation included the airspeed, engine torque, propeller shaft speed, aircraft angle of attack, and the wing upwash angle. The criteria used for the identification of the three ground operation categories are summarized in table 5.

Table 5. Summary of Criteria Used for the Identification of the Ground Phases

Phase	Starting Criteria	End Criteria
General Ground Operations	IAS <84 kt	IAS >84 kt
Takeoff Roll	IAS >50 kt and increasing	Liftoff or IAS decreases
Reverse Propeller	Reverse parameter indicates propeller in reverse	Reverse parameter indicates propeller not in reverse

5.5.2 Flight Operations.

As indicated in figure 5, flight operations were divided into five phases: (1) departure, (2) climb, (3) cruise, (4) descent, and (5) approach. The separation criteria used for the five flight phases are summarized in table 6. It should be noted that an airborne phase could occur several times per flight.

Table 6. Summary of Criteria Used in the Identification of the Five Flight Phases

Phase	Start Criteria	End Criteria
Departure	Takeoff rotation and flaps extended	Flap retraction
Climb	VS >750 fpm for 20 s (flaps up; IAS >101 kt)	VS <750 fpm for 20 s
Cruise	|VS| ≤200 fpm for 20 s (flaps up; IAS >101 kt)	Δh >250 ft for 20 s from average altitude of first 20 s of cruise
Descent	VS <-750 fpm for 20 s (flaps up; IAS >101 kt)	VS >-750 fpm for 20 s OR flaps extended for 20 s OR IAS <101 kt for 20 s
Approach	Flap extension at IAS >101 kt	IAS <84 kt or flap retraction

VS = Vertical speed

The departure phase started immediately after the takeoff rotation with the flaps extended. The departure segment was characterized by a positive rate of climb. In the few cases where flaps were not used for takeoff, the climb phase was assumed to commence very shortly after the takeoff rotation. A flap retraction marked the end of the departure phase.

The start of a climb phase was characterized by a rate of climb greater than 750 feet per minute (fpm) for 20 seconds with the flaps retracted. The end of climb was marked when the vertical speed decreased below 750 fpm for 20 seconds.

The beginning of the cruise segment was marked by the vertical speed value remaining within ±200 fpm for 20 seconds. The average altitude during the first 20 seconds of a cruise was used to determine the termination point of this phase. When the difference between this average value and the altitude of the aircraft remained greater than 250 feet for at least 20 seconds, the cruise segment was assumed to end.

A rate of descent that remained greater than 750 fpm for 20 seconds with the flaps retracted marked the start of a descent phase. Unlike a climb segment, this phase required multiple ending criteria as this phase could be followed either by a cruise, an approach, or possibly even a landing without flaps. To account for the three possible scenarios, this phase was terminated if either the rate of descent was below 750 fpm for 20 seconds and the flaps were deployed and remained extended for 20 seconds or if the airspeed remained below 101 knots for 20 seconds.

Approach started when the flaps were deployed at an indicated airspeed greater than 101 knots. The aircraft had a stalling speed of 101 knots with the gear and flaps retracted, and since a weight-on-wheel parameter was not recorded, the 101 knots airspeed helped to ensure the aircraft was in the air at flap deployment. The end of approach occurred when the indicated airspeed decreased to less than 84 knots, indicating a landing, or upon the retraction of the flaps as would occur during a go-around procedure.

5.6 METHODS OF DATA EXTRACTION.

5.6.1 Ground Operations.

5.6.2 Operations Within Prohibited Shaft Speed Range.

While on the ground, stabilized operation within propeller shaft speed ranges from 400-950 rpm and 1250-1395 rpm is prohibited. When the shaft speed was within one of these ranges, the length of time it remained within that range was saved. All of the saved times greater than 5 seconds were added together to arrive at the total time the propellers were operated in the restricted zones for more than 5 seconds. The same was done for periods greater than 10, 15, 20, 25, and 30 seconds, respectively. This value was extracted for the purpose of comparing it to the time values discussed above. The reason for the different time cut-offs was that the length of time associated with "stabilized" operation was not known.

During normal operations, the propeller shaft speed has to transition through these restricted bands, and therefore, the duration of the transitions through these ranges was of interest. Transition was defined as the shaft speed crossing the restricted zone while increasing or decreasing. If the shaft speed entered and exited a band from the same side, it was not considered to be a transition. The absence of a clear definition of "stabilized operation" came into play again with the restricted zone transitions. There were cases where a slow transition through one of these ranges was counted as a stabilized operation due to its total duration. A 60-second time limit was used as a maximum duration for transitions. Transitions characterized by increasing shaft speeds were separated from those with decreasing shaft speeds.

5.6.2.1 Propeller Shaft Speed Before Engine Shutdown.

One of the characteristics of the recorded engine data was that the propeller shaft speed assumed a negative value when the engine was not running. The shaft speed at idle was observed in the data files to remain around 1000 rpm, but it plummeted to a negative value at shutdown. Accordingly, propeller shaft speed before shutdown was found by first locating the time when the shaft speed became negative. Stepping back from this time, the time when the difference between two consecutively recorded values was less than 20 rpm was found. The rpm at this point was labeled as the propeller shaft speed before engine shutdown.

5.6.2.2 Propeller Reversal.

The data indicated that propeller reversal was used upon landing and during ground maneuvering. In this setting, the propellers are loaded in a direction opposite to the loading they experience during the majority of operation. Furthermore, propeller reversal increases the potential for propeller buffeting due to high power settings and boundary layer separation over the blades [5]. Due to these factors, the reverse cycle is an important part of the propeller loading spectrum in terms of fatigue life and flutter potential [5 and 6].

Factors that influence the severity of the loads on the propeller during a reverse cycle are the engine torque, propeller shaft speed, and the airspeed at which this event occurs. Propeller reversal was recorded as a discrete parameter in the data files. When this parameter indicated

that the propeller was in reverse, the maximum and minimum shaft speeds and engine torque during this phase were recorded. The indicated airspeed at the start of a propeller reversal and the duration of the reverse cycle were recorded.

5.6.2.3 Takeoff Rotation.

Identification of the takeoff rotation followed from that of the takeoff roll. The pitch attitude was averaged over the takeoff roll, and a change of more than 2 degrees from the average value was labeled as the start of the takeoff rotation. This was not necessarily the point of liftoff, but rather, the point where the rotation for takeoff was initiated. In the few seconds following this rotation, the maximum angle of attack, and accordingly the greatest inflow angle into the propeller disk would be reached. Accordingly, the point of maximum angle of attack within the 10 seconds after the start of the takeoff rotation was called the point of liftoff. At the liftoff point, the aircraft might have been a few feet off the ground, but this point would coincide with the maximum inflow angle and thus was of interest. This large inflow angle would lead to the highest 1P loads on the propeller blades.

5.6.3 Flight Operations.

5.6.3.1 Flap Operations.

A change in the wing flap position results in a change in the upwash angle ahead of the wing as well as a change in the aircraft angle of attack. The upwash angle arises from the curvature of the streamlines upstream of a lifting system. These changes affect the propeller inflow angle and consequently, the 1P loads on the propeller blades. Flap operations at high power settings were of particular interest as the loads on the propellers were already high, and a change in inflow angle would have a more pronounced effect on blade loading. Generally, high power settings were used during takeoff, departure, and go-around, when the flaps would only be retracted from an initially deployed position.

The only parameter studied was the airspeed at which flap retraction occurred. The BE-1900D has three flap positions—up (0º), approach (17.5º), and down (35º)—and the stalling speed of the aircraft with flaps in the respective positions is 101, 90, and 84 knots [12 and 13]. This information is summarized in table 7. When the flap position indicator changed from down to approach at airspeeds greater than 90 knots, or from approach or down to up at airspeeds above 101 knots, a flap retraction was assumed. The flaps had to be in one position for 3 seconds before retraction and then remain in the new position for another 3 seconds for the operation to be considered a flap retraction. The 3-second time limit eliminated erroneous flap position readings that occurred randomly in some of the data files. The airspeed limits ensured the aircraft was in the air when the retraction occurred. Once the change in flap position was determined to be a valid retraction, the indicated airspeed at which the flap retraction occurred was recorded.

Table 7. BE-1900D Flap Detents

Flap Detent	Flap Setting	Operational Placard Speed (KIAS)	Stall Speed (KIAS)
0	Retracted	248	101
1	Half	188	90
2	Full	154	84

5.6.3.2 Torque and Thrust Correlated With Propeller Shaft Speed.

The maximum torque the PT6A-67D engine can produce is 3950 ft-lbf, and 100% propeller shaft speed is equal to 1700 rpm [13]. To obtain the in-flight torque versus propeller shaft speed data, the torque was divided into 20 bands, 18 of which were equally sized between 0 and 3600 ft-lbf. The next band spanned from 3600 to 3750 ft-lbf, and the final band included all torques greater than 3750 ft-lbf. The maximum continuous torque limit on the BE-1900D engines is 3750 ft-lbf, and operation at torque levels greater than 3750 ft-lbf (takeoff power) is limited to 5 minutes [13]. Therefore, the final two bands were sized to include the maximum continuous torque limit. Propeller shaft speed was also separated into 20 bands between 800 and 1800 rpm. The maximum of 1800 rpm was used since this parameter was regularly observed to be between 1700 and 1800 rpm during high power operations (i.e., takeoffs). Another reason for this upper limit was the maximum propeller over-speed limit of 110%, or 1870 rpm, which meant shaft speeds greater than 1700 rpm were possible [13]. Whenever a combination of a torque and shaft speed band occurred, that combination was incremented by one. In essence, the number of occurrences of each torque and shaft speed combination was found. Knowing each occurrence lasted 1 second, the total time in that combination was determined. Therefore, the number of occurrences was converted to a percentage of the total flight time.

5.6.3.3 Time Versus Airspeed and Torque.

The time spent operating at various airspeed and torque levels was examined to understand the basic operation of the aircraft. Indicated airspeed was grouped into bands 20 knots wide, spanning between 100 and 260 knots; a ninth band spanned from 84 to 100 knots to account for the aircraft stalling speed. The torque was divided into bands between 0 and 3200 ft-lbf with bandwidths of 400 ft-lbf. Two final bands of unequal size were used again to include the maximum continuous torque limit of 3750 ft-lbf. The number of occurrences of each band was counted, and since indicated airspeed and engine torque was recorded at 1 Hz, each occurrence corresponded to one second at that airspeed or torque level. Thus, the number of occurrences matched directly to the total number of seconds spent operating within each band.

5.6.4 Sign Convention.

Vertical acceleration was considered positive upward. Vertical gust speed was considered positive if it caused a load factor greater than unity.

5.6.5 Separation of Maneuver and Gust Load Factors.

The incremental acceleration measured at the center of gravity of the aircraft may be the result of either maneuvers or gusts. To derive gust and maneuver statistics, the maneuver-induced accelerations and gust response accelerations had to be separated from the total acceleration history. Reference 8 reports the results of a UDRI study to evaluate methods of separating maneuver and gust load factors from measured acceleration time histories. As a result of this study, the Federal Aviation Administration (FAA) recommended and accepted that a cycle duration rule be used to separate gusts and maneuvers. A cycle duration of 2.0 seconds was recommended for Boeing 737 and McDonnell Douglas 82/83 aircraft. Review of the BE-1900D response characteristics has shown that this cycle duration can also be used with the BE-1900D data.

5.6.6 Peak-Valley Selection.

While examining gust and maneuver loads, the peak-between-means method of reference 7 was used to select the peaks and valleys in the acceleration and derived gust velocity data. This method is consistent with past practices and pertains to all accelerations, whether due to gusts or maneuvers. In this method, only one peak or valley is counted between two successive crossings of the mean. A threshold zone (deadband) is used in the data reduction to ignore irrelevant load variations around the mean. This is shown schematically in figure 6. The same deadband values were used for gusts and maneuvers. The deadbands associated with the loads and the derived gust velocity are shown in table 8.

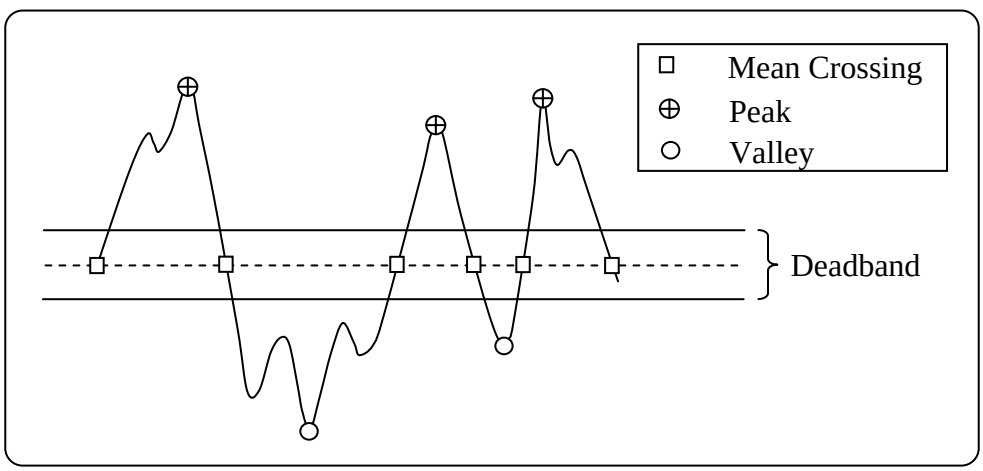

Figure 6. Peak-Between-Means Classification of Loads

Table 8. Peak-Valley Deadband Limits

Parameter (Units)	Deadband Width
Incremental vertical acceleration (g)	±0.050
Derived vertical gust velocity (ft/s)	±2.00
Gust-induced change in angle of attack (degree)	±0.10

From derived gust velocities, instantaneous changes in angle of attack were determined. A deadband between ±0.1 degree from the mean was established to eliminate small variations due to the inherent noise in the data. A $\Delta\alpha$ that remained either above or below the deadband for more than 2 seconds was assumed to be due to a maneuver, and anything less than 2 seconds due to a gust. When a $\Delta\alpha$ was determined to be due to a gust, the maximum (peak) above the deadband or minimum (valley) below the deadband was determined. The peaks and valleys were then sorted into bins of $\Delta\psi$ that had widths of 0.1 degrees and spanned from -6 to +6 degrees. The number of occurrences of the peaks and valleys was found and categorized according to the flight phase (climb, cruise, or descend) during which they occurred.

5.6.7 Altitude Bands.

The number of occurrences of peaks and valleys of the gust-induced angle of attack was separated into the altitude bands shown in table 9, with finer divisions at lower altitudes where turbulence is typically more prominent.

Table 9. Altitude Bands Above Airports

Bands	Altitude Above Sea Level (ft)
1	<500
2	501-1,500
3	1,501-4,500
4	4,501-9,500
5	9,501-14,500
6	14,501-19,500
7	19,501-24,500

6. DATA PRESENTATION.

6.1 OVERALL AIRCRAFT USAGE.

This section presents data that depicts the usage of the aircraft and some of its systems. An understanding of the overall usage will aid in the comprehension of the data presented in the following sections. This section does not present data that is necessarily directly related to the propeller usage and loads, but rather, more general operational data. Data such as the individual flight durations, the time spent in different flight phases, and the flap usage will be shown in the following section.

6.1.1 Flight Duration and Distance.

Figure 7 shows the flight duration distributions. The average flight lasted about 39 minutes, with standard deviation of 17.5 minutes. A significant number of flights fell within the 5- to 10-minute range. These short flights could possibly be the result of post-maintenance test flights where the aircraft remained within the traffic pattern or even came from short-hop flights from small airports nearby a larger one. From the data in this figure, one can derive the average flight

distance to be about 150 nautical miles. The short distances flown by these aircraft show the nature of commuter airline flights. Also, these short flight durations mean that these aircraft go through multiple flight cycles much more rapidly than a long-haul airliner would. Accordingly, subsystems, such as the landing gear, flaps, engines, propellers, as well as the aircraft structure, experience many loading cycles within the operational life of these aircraft.

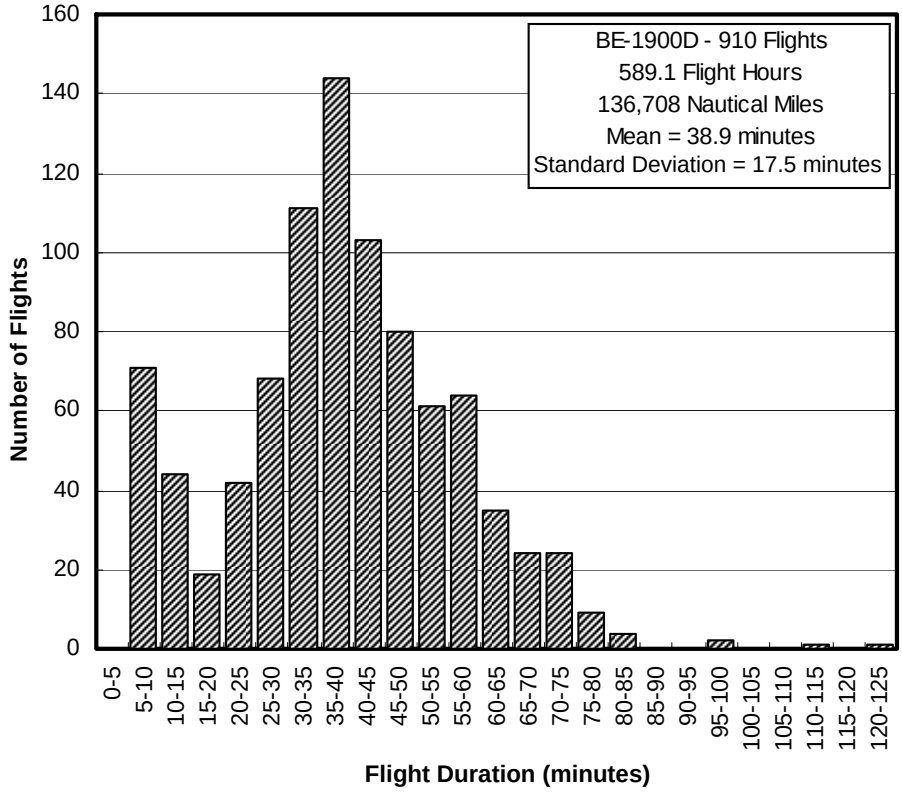

Figure 7. Number of Flights Versus Flight Duration

Figure 8 presents the percentages of the total flight time and flight distance spent within each of the five flight phases. Departure, climb, and approach show a smaller distance percentage than time percentage, whereas cruise and descent show a larger distance percentage than time percentage. The reason for this is that cruise and descent were characterized by higher airspeeds than the other three phases, thus, exhibited higher distance percentage. The lower flights' speed with the flaps deployed means the aircraft spends a larger percentage of time in departure, climb, and approach.

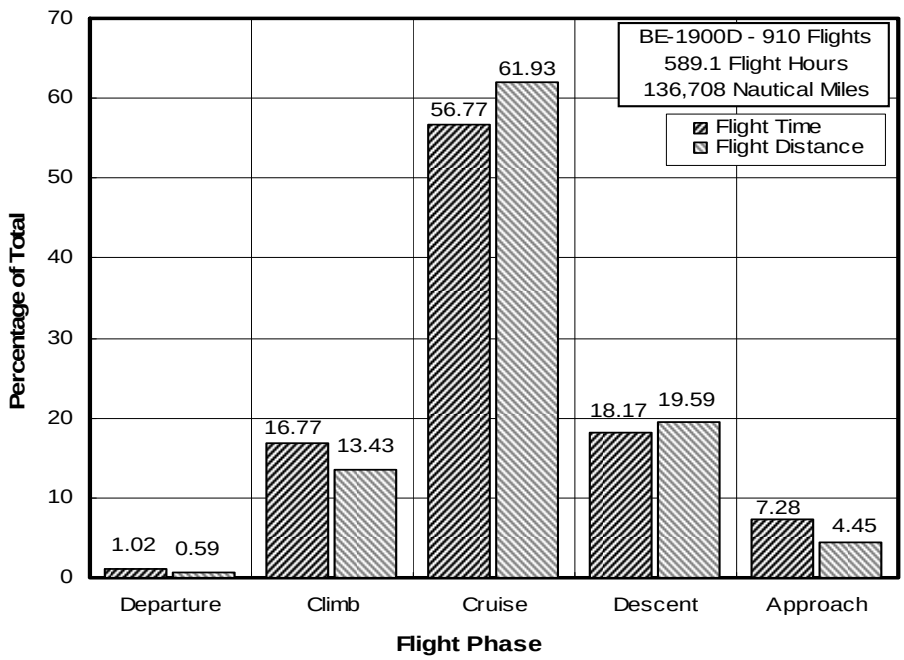

Figure 8. Percentage of Total Flight Time and Flight Distance per Flight Phase

Figure 9 shows the percentage of time spent at the different airspeeds. The aircraft cruised at airspeeds between 200 and 240 knots, which were maintained during descents. This explains the large percentage of operation within this range. Rarely did the aircraft exceed the maximum operating speed of 248 knots. The other high point in figure 9, around the range of 160 to 180 knots, is the airspeed at which the aircraft climbed.

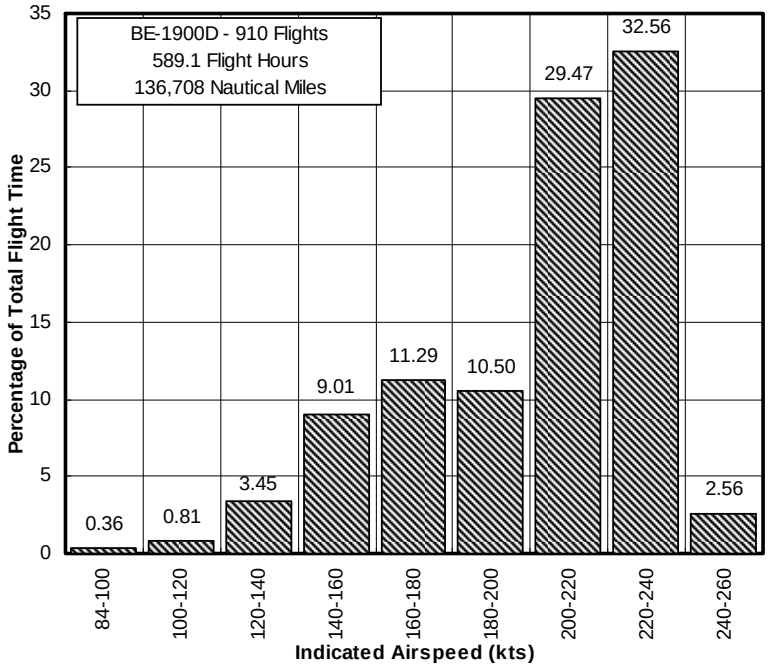

Figure 9. Percentage of Total Flight Time Operating at Different Airspeeds

6.1.2 Flap Usage.

6.1.2.1 Takeoff and Landing.

Flap usage is part of both takeoff and flight operations, and also falls under the category of systems usage. Figure 10 shows the percentage of takeoffs and landings performed with the flaps in various positions. The majority of takeoffs were performed with the flaps in the approach position, and only a small percentage of takeoffs were performed with full flaps or no flaps. The reason for using full flaps for takeoff is not clear, but this would potentially reduce the acceleration of the aircraft due to higher drag forces. A takeoff performed without flaps could have been done at airports with longer runways where the aircraft would have been able to accelerate to higher airspeeds before liftoff. Landings were mostly executed with the flaps in the down position, but a few were performed with the flaps in the other two positions. Flaps help to decelerate the aircraft, reduce the stalling speed of the aircraft, lower the pitch angle to aid in forward visibility for the pilots during the final stages of an approach, and reduce the touchdown speed of the aircraft upon landing. Thus, landings with flaps in a position other than down were unanticipated.

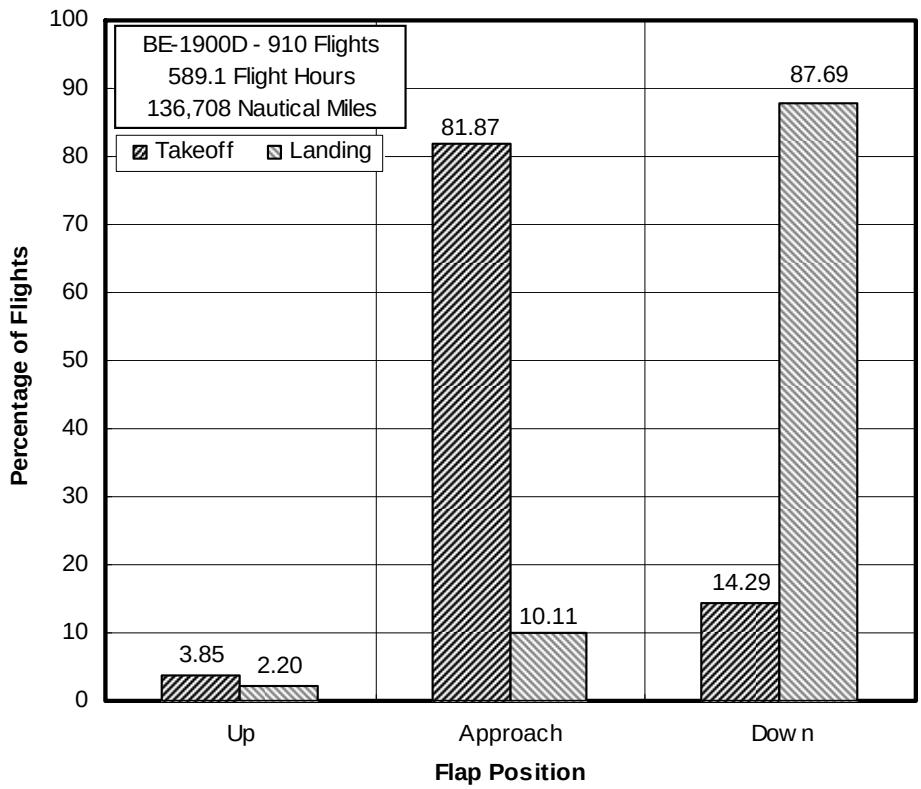

Figure 10. Percentage of Takeoffs and Landings Performed With Flaps Deployed

6.1.2.2 Airspeed at Flap Retraction.

Figure 11 shows the distributed and the cumulative probability of airspeed at flap retraction. In this case, a beta distribution was most suitable to present the data. All of the flap retractions

occurred at airspeeds greater than 120 knots with an average airspeed of about 145 knots. A significant number of flap retractions occurred at airspeeds greater than 154 knots, but since the bulk of takeoffs were performed with the flaps in the approach position, the flaps were likely in the approach position at these higher airspeeds. Few retractions occurred at airspeeds greater than 188 knots.

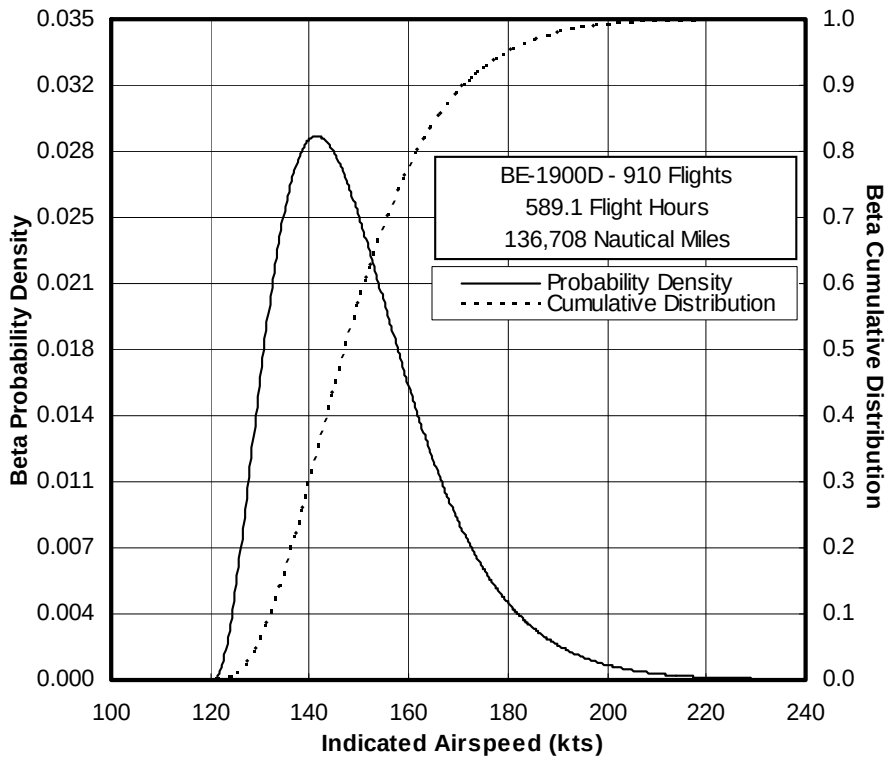

Figure 11. Beta Probability Density and Cumulative Distribution of the Airspeed at Flap Retraction—a = 120.41, b = 9.447E+7, α_1 = 3.467, α_2 = 1.108E+7

6.1.2.3 Percentage of Flights With Flaps Deployed.

The percentage of total flight time with the flaps in the different positions is shown in figure 12. Since the flaps are used mostly for departure and approach, a very small percentage of flight time was performed with the flaps deployed.

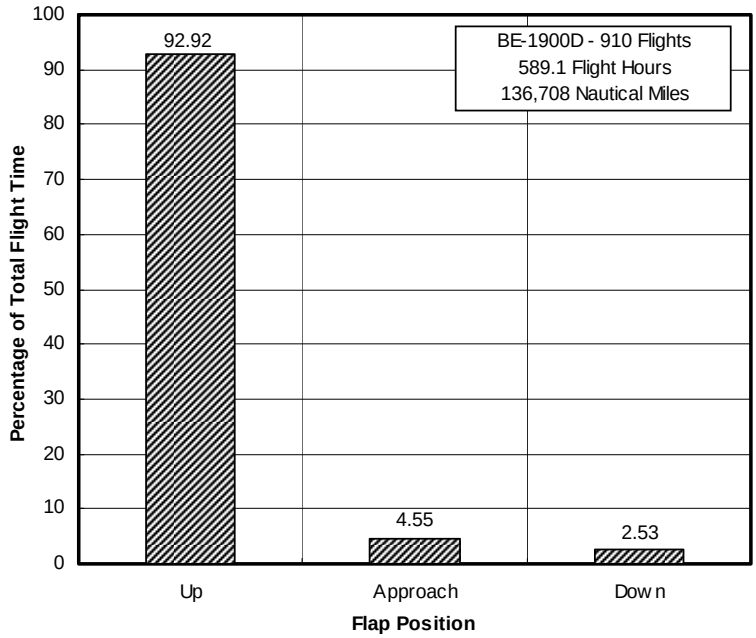

Figure 12. Percentage of Total Flight Time With Flaps Deployed

6.1.3 Overall Engine Usage.

The percentage of time the engines were operated in different torque bands is shown as a percentage of the total flight time in figure 13. Very little time was spent at torque levels greater than the maximum continuous limit of 3750 ft-lbf (0.22%, equivalent to about 5 seconds per flight). The vast majority of the flight time was spent at torque levels between 2800 and 3750 ft-lbf.

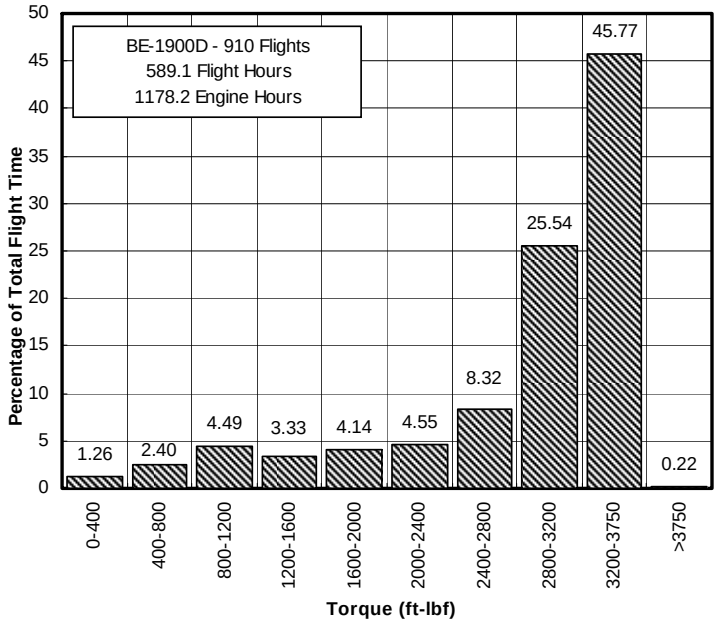

Figure 13. Percentage of Total Flight Time at Different Torque Levels

6.2 GROUND OPERATIONS.

6.2.1 General Ground Operations.

The parameters studied under the general ground operations category included the propeller shaft speed before engine shutdown, stabilized operations within the restricted propeller shaft speed ranges, and transitions through the restricted ranges.

6.2.2 Shaft Speed Before Shutdown.

Propeller shaft speed before engine shutdown is shown in figure 14. The idling shaft speed of the propellers is about 1000 rpm. The shaft speed before shutdown fell within a very narrow band around 1000 rpm. A significant number of shutdowns, approximately 20%, occurred from a shaft speed below 950 rpm, which means the propellers were within the lower prohibited operating range. However, this is not necessarily the same as stabilized operation within the restricted zone.

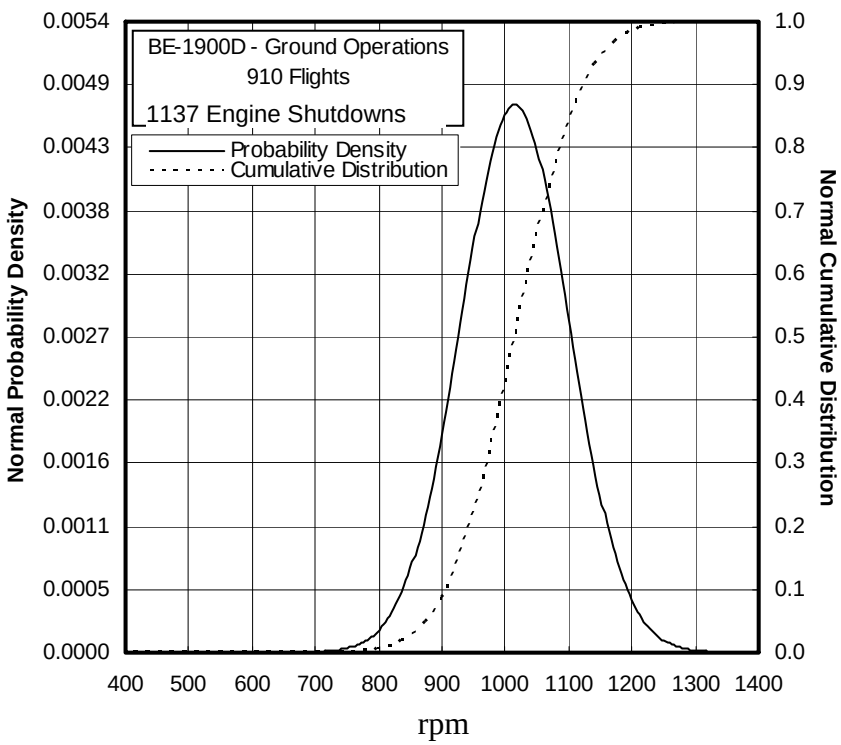

Figure 14. Distributed and Normal Probability Density of rpm Before Engine Shutdown
μ = 1015 rpm, σ = 85.1 rpm

6.2.3 Operations Within Restricted Zone.

Operations within the restricted propeller shaft speed ranges were closely scrutinized. These ranges spanned from 400 to 950 rpm and 1250 to 1395 rpm. Due to the lack of a clear definition of "stabilized ground operations," operations within the prohibited range for various durations were found. The data for the lower rpm range is shown in figure 15. A surprisingly large

percentage of time was spent within this lower prohibited range. Since a typical idling shaft speed was approximately 1000 rpm, the propellers possibly spent excessive time idling just within the lower restricted band. This conclusion is supported by the observation that 75% of the total length of time in the lower restricted band came from being within that range for more than 30 seconds. The result from engine shutdowns also supports this hypothesis.

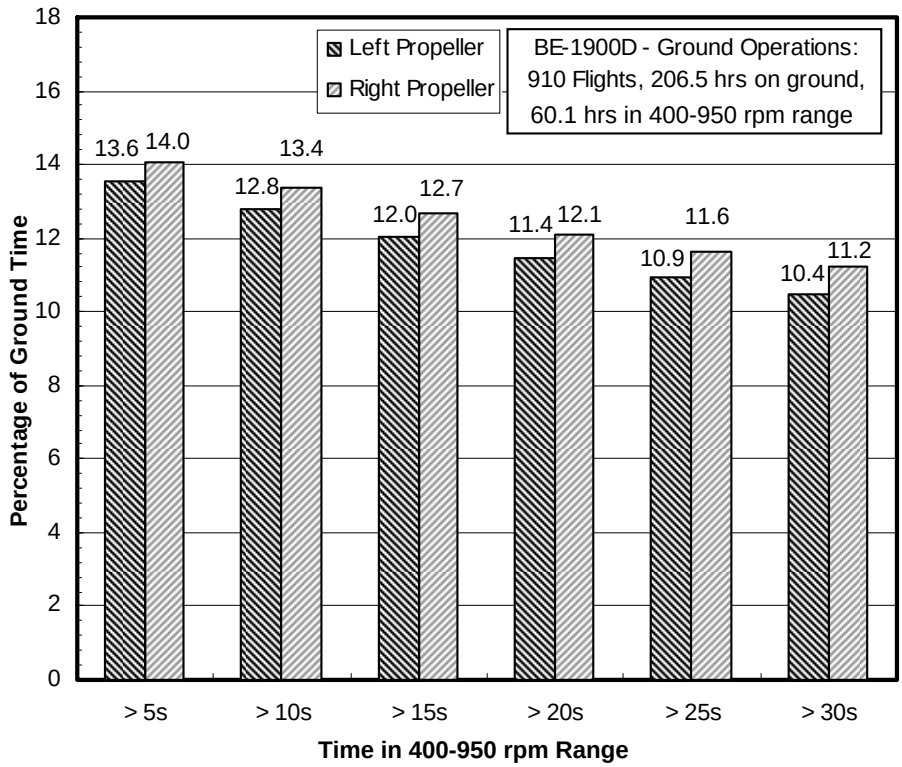

Figure 15. Percentage of Time Operating in the 400 to 950 rpm Range

Figure 16 shows that much less time was spent operating within the upper restricted range. This figure supports the reason given for the large length of time spent within the lower band as well. Both figures 15 and 16 show a shorter time for the left engine than the right. The data showed that at the end of many flights, only the left engine was shutdown. This was probably done to load or unload without complete shutdown or to reduce fuel burn by taxiing with one engine.

The time to transition through a restricted propeller shaft speed range was also studied since crossing these zones is part of normal operations. Lognormal distributions of the increasing and decreasing shaft speed transitions are shown in figure 17. The majority of transitions lasted less than 10 seconds. Increasing transitions were generally slower than the decreasing transitions. This disparity between increasing and decreasing transitions appear to be a valid result considering the engine has to overcome aerodynamic drag to increase the shaft speed; whereas, the propellers just have to slow with the drag force for decreasing transitions. Many of the transitions are also likely to have been a result of engine shutdowns when the propellers go into a feathered position due to the loss of oil pressure. This causes a rapid decreasing propeller shaft speed caused by the very high propeller pitch angle and resulting high drag.

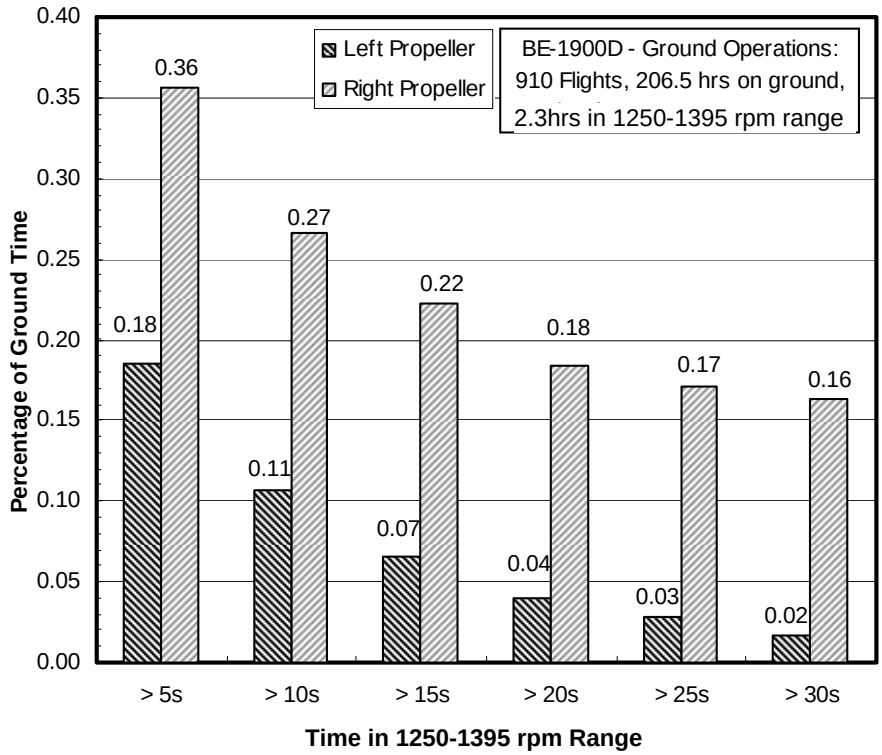

Figure 16. Percentage of Time Operating in the 1250 to 1395 rpm Range

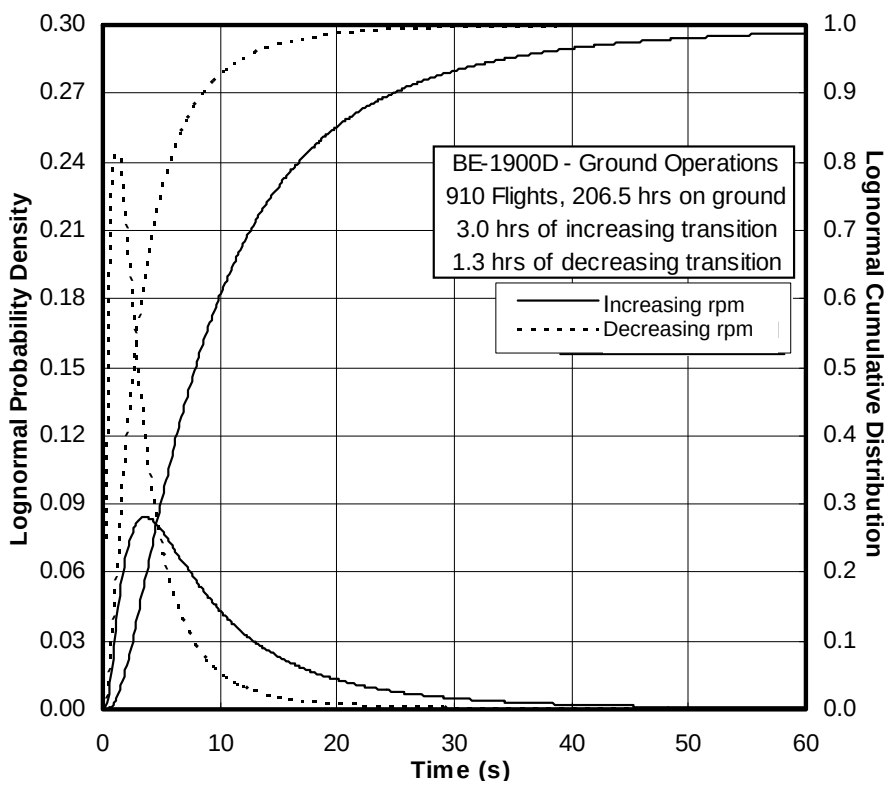

Figure 17. Time to Transition Through Restricted Propeller Shaft Speed Ranges
Increasing rpm: $\mu = 2.067$, $\sigma = 0.890$—Decreasing rpm: $\mu = 0.999$, $\sigma = 0.903$

Other than the difference in duration of the two transition types, a contributing factor to the total time difference is the increase of shaft speed at the start of a takeoff run. This transition was captured under general ground operations, whereas the decrease of the shaft speed through the upper prohibited range upon landing would not. During landing, the transition takes place, or at least start, above 84 knots indicated airspeed and thus, would not have been captured under the general ground operations.

6.2.4 Propeller Reversal.

The primary purpose of reverse thrust is to brake after landing. Therefore, it was expected that reverse thrust would have been used during all landings, as this would greatly reduce the wear of the wheel brakes and tires.

Table 10 shows the occurrences of reverse thrust used after landing. In the absence of a squat switch recording, landings were identified from the airspeed. Based on the stall speed, if the airspeed decreased from 110 to 100 KIAS and was below 84 KIAS 15 seconds later, then a landing was assumed. The propeller reversal parameter was checked for 20 seconds after landing to ensure capturing the entire landing roll out.

Table 10. Use of Reverse Thrust After Landing

Reversal After Landing	Number
Left propeller only	121
Right propeller only	33
Both propellers	320

The data in table 10 shows that in a large number of cases, only one propeller was reversed. It is unlikely that these cases were associated with braking after landing. Since in practice, most landing rolls are shorter than 20 seconds, it is more likely that most of the one-sided reversals occurred a short time after the completion of the landing roll and were associated with taxiing after landing.

Both propellers were reversed after landing in only 320 of the 910 landings, indicating braking. In the majority of these cases, the data regularly showed that one propeller went into reverse about 1 to 2 seconds before the other. It is unclear if this trend was due to the sensor installation and calibration, or if it truly indicated asynchronous reversal. However, there are anecdotal references to the latter among pilots familiar with BE-1900D.

The results obtained from extracting the indicated airspeed at the start of the reverse cycle is shown in figure 18. The total number of reverse cycles (2091) indicated in this figure is the sum of the events for both left and right propellers. This figure clearly shows that propeller reversal was used for two separate purposes, one at airspeeds below 50 knots and another at approximately 80 knots. The minimum recorded airspeed varied from one data file to the next, but the minimum was always less than 50 knots. Thus, the high concentration of reversals at airspeed below 50 knots represents reverse thrust usage during taxi and ground maneuvering. Due to the varying minimum recorded airspeed, the airspeeds below 50 knots in figure 18 do not

represent the true airspeeds of the aircraft at the time of those reversals. The cluster of events on the right was due to braking after landing, which typically occurred at airspeeds between 70 and 90 knots.

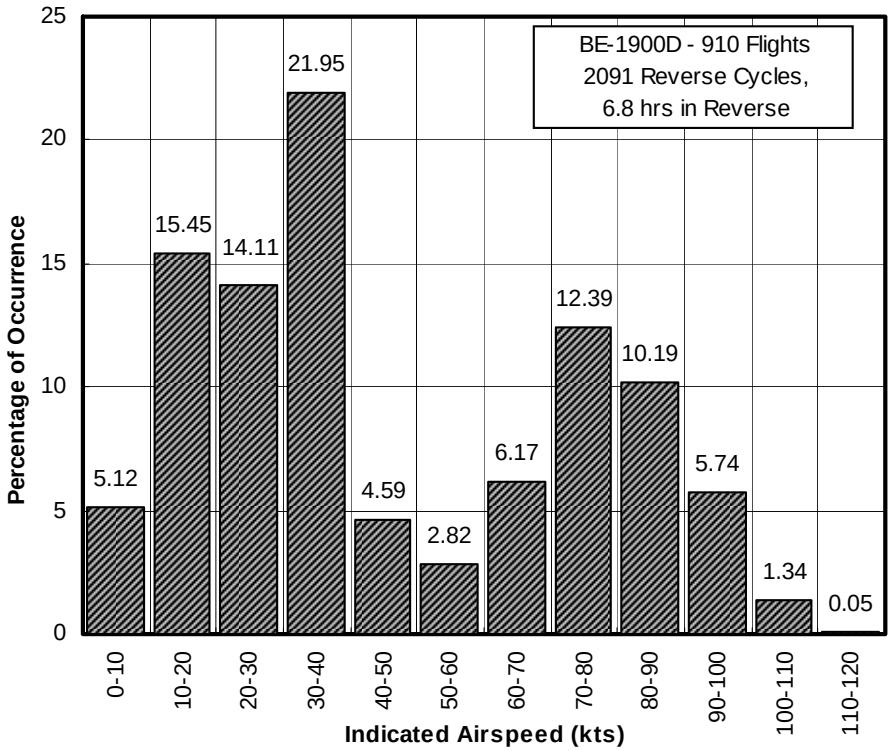

Figure 18. Indicated Airspeed at Start of Propeller Reversal

The data revealed that reversals of the left and right engines did not necessarily correlate during ground operations. This may have been done to aid in the ground maneuvering of the aircraft. One propeller producing reverse thrust while the other produces forward thrust would allow the aircraft to make a very small radius turn. In addition, using thrust reversal to turn and brake the aircraft on the ground decreases brake wear. Reversals upon landing, on the other hand, were usually well correlated between the left and right propellers, except for the small time difference at the start of the reversals mentioned earlier.

Figure 19 shows a lognormal distribution of the duration of the reverse cycles. Reversals generally lasted for less than 10 seconds and those lasting longer than 20 seconds occurred very rarely. Reversals upon landing were not expected to last more than 10 seconds as landing rollouts are short-duration events. The same was true for reversals while taxiing, as reverse thrust would generally be used to brake or turn the airplane and, thus, be of short duration.

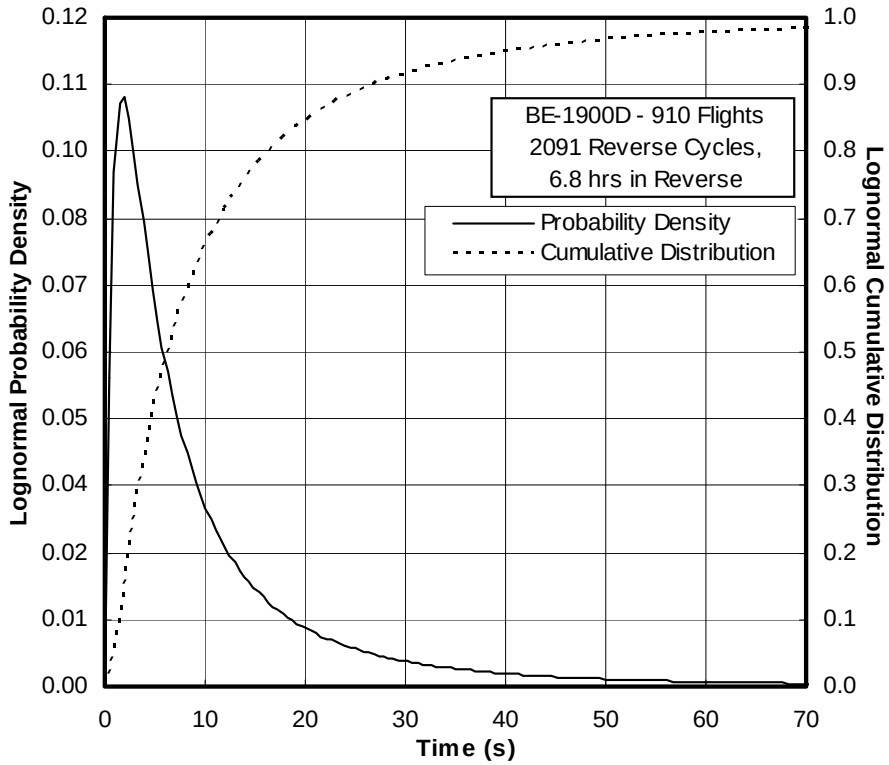

Figure 19. Distributed and Cumulative Lognormal Probability of Reverse Cycles Duration
$\mu = 1.841$, $\sigma = 1.133$

Figures 20 and 21 present the probabilities of the maximum and minimum propeller shaft speed and engine torque during a reverse cycle. Figure 20 shows a difference between the maximum and minimum shaft speeds of about 100 rpm and an average reverse propeller shaft speed of about 1050 rpm. The maximum engine torque during a reverse cycle was only slightly higher than the minimum, with the majority of reversals happening with the torque less than 500 ft-lbf. Few reversals occurred with torques greater than 1500 ft-lbf.

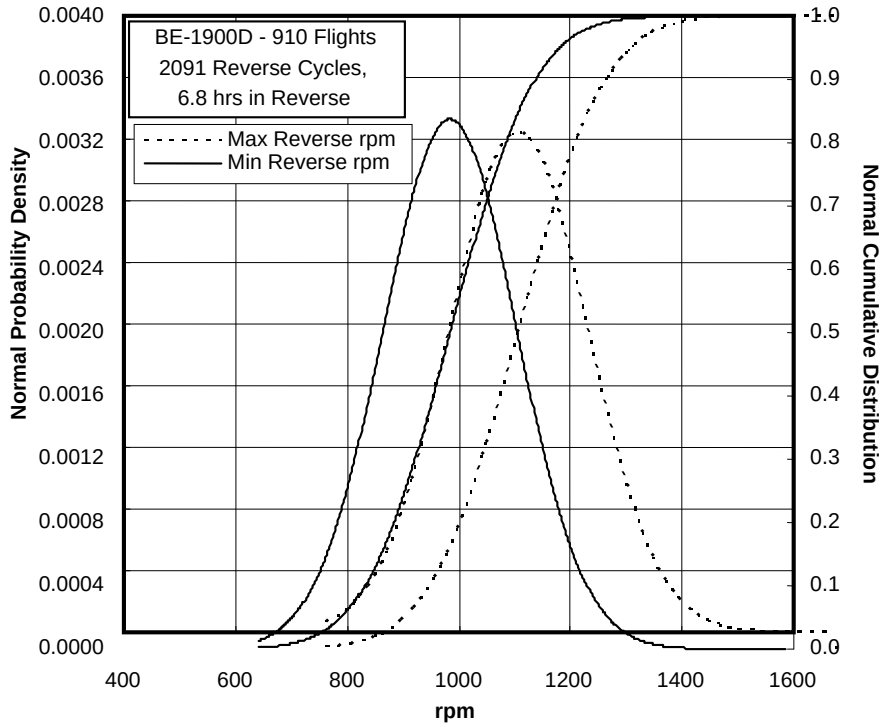

Figure 20. Distributed and Cumulative Normal Probability of rpm at Propeller Reversal
Maximum: $\mu = 1107.0$, $\sigma = 123.16$—Minimum: $\mu = 984.32$, $\sigma = 119.08$

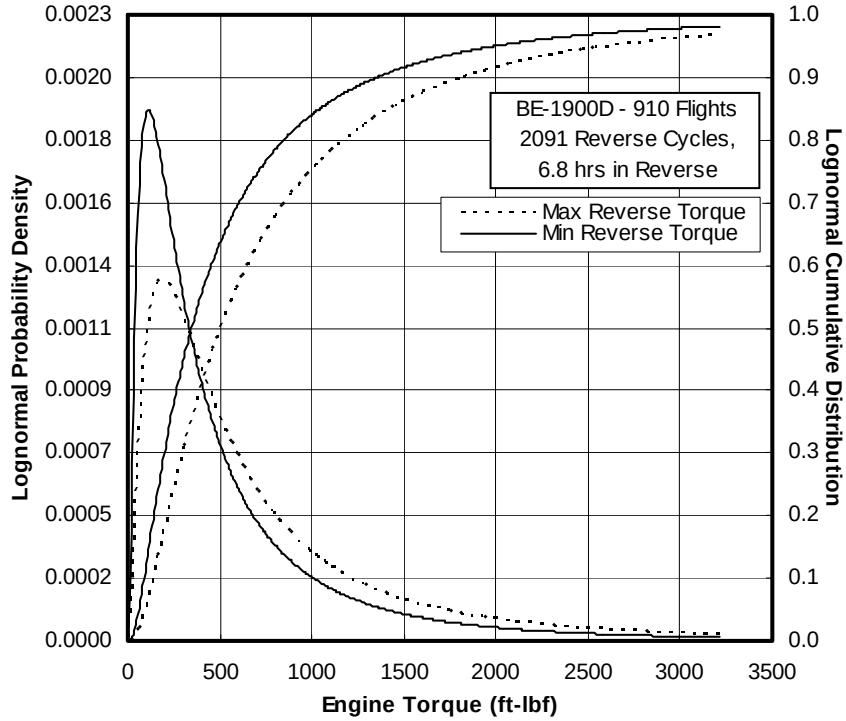

Figure 21. Distributed and Cumulative Lognormal Probability of Torque at Propeller Reversal
Maximum: $\mu = 6.229$, $\sigma = 0.996$—Minimum: $\mu = 5.846$, $\sigma = 1.063$

6.2.5 Takeoff Rotation.

6.2.5.1 Propeller rpm and Torque.

Takeoff rotation was deemed to be one of the most demanding segments of operation for the propeller blades due to the high inflow angle coupled with high power settings. Figures 22 and 23 show the propeller shaft speed and engine torque, respectively, at rotation. Full power was generally used for takeoffs, evident in these figures from the mean 1725 rpm and 3500 ft-lbf of torque at rotation. The airspeed at takeoff rotation also affects the severity of the 1P loading the blades experience. Normal probability of this parameter is presented in figure 24. Takeoff rotation typically occurred around 112 knots or a dynamic pressure of about 42.5 psf. Rotation does not necessarily correspond with the liftoff point; thus, when rotations occurred at lower airspeeds, it did not mean the aircraft lifted off the ground at those airspeeds.

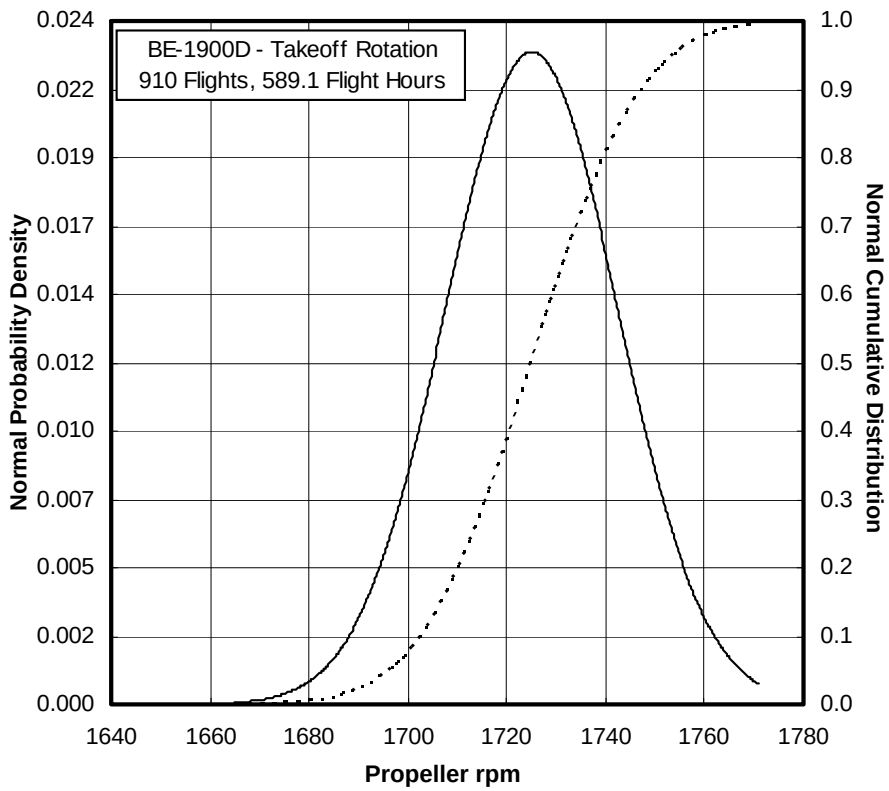

Figure 22. Distributed and Cumulative Normal Probability of rpm at Takeoff Rotation
$\mu = 1725.0$, $\sigma = 17.41$

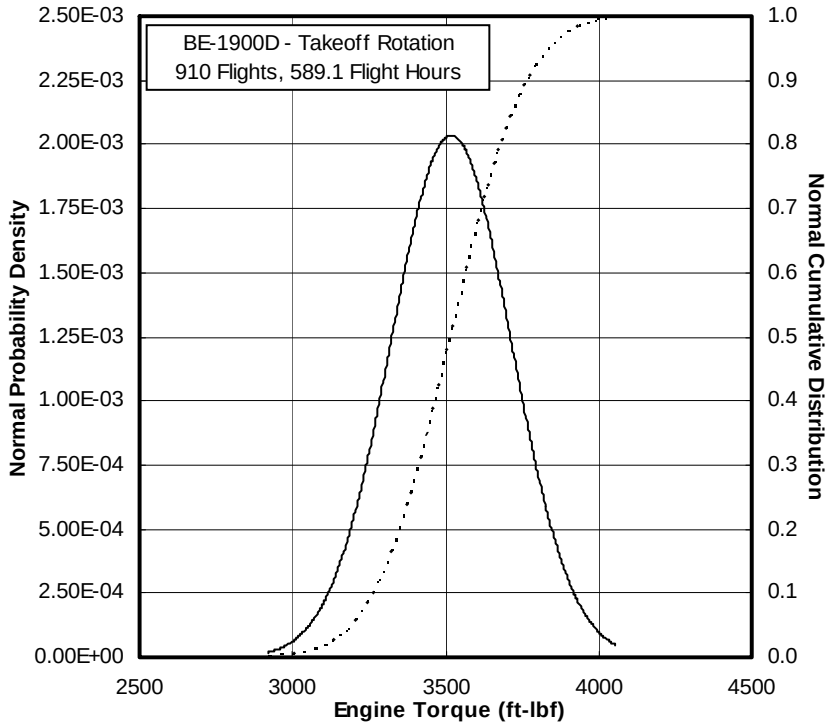

Figure 23. Distributed and Cumulative Normal Probability of Torque at Takeoff Rotation
$\mu = 3518.0$, $\sigma = 195.98$

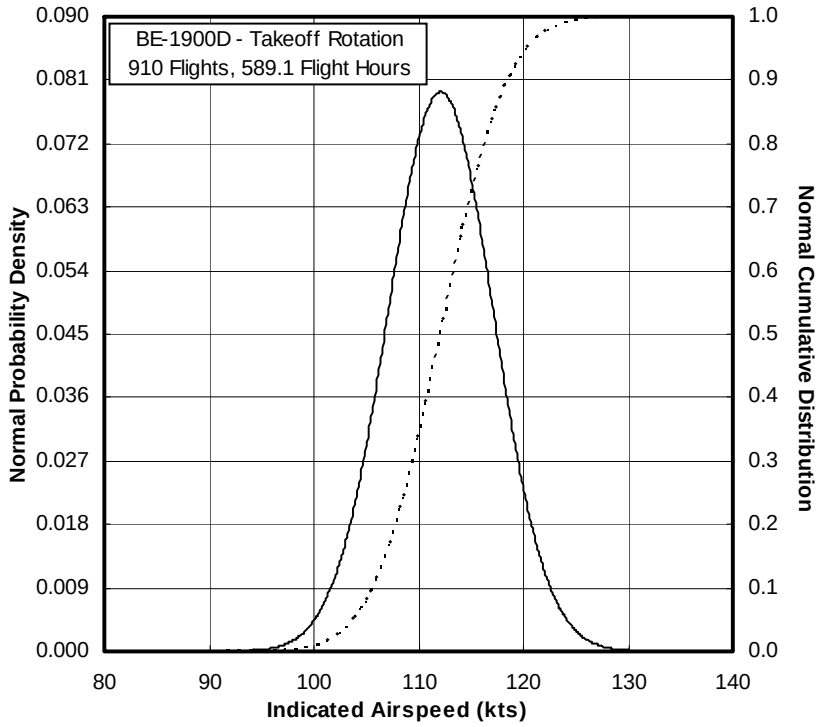

Figure 24. Distributed and Cumulative Normal Probability of Airspeed at Takeoff Rotation
$\mu = 112.11$, $\sigma = 5.029$

6.2.5.2 Liftoff Angle of Attack.

Distributed and cumulative normal probability of the angle of attack at liftoff is presented in figure 25(a) and (b). Takeoffs were categorized by the three flap positions. The average liftoff angle of attack of the takeoffs performed with full flaps was smaller than those with either approach or no flaps. Considering the sample sizes, this result is considered reliable. Approach flaps lessened the liftoff angle of attack from the no flaps case as was expected. However, only 35 no flaps cases were extracted in contrast to the 745 approach flaps cases. As a result of the small sample size, the data for no flaps cases is considered to be unreliable. A larger number of no flaps takeoff cases would have to be studied for conclusive and reliable results.

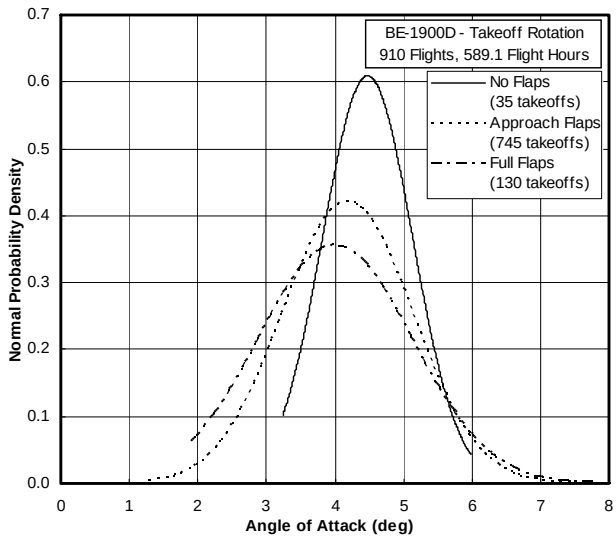

(a) Probability Density

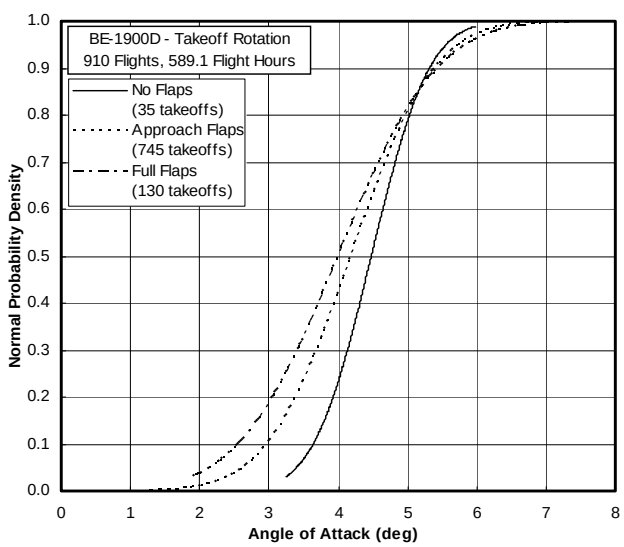

(b) Cumulative Distribution

Figure 25. Normal Probability of Angle of Attack at Liftoff,
No Flap: $\mu = 4.48$, $\sigma = 0.66$—Half Flap: $\mu = 4.18$, $\sigma = 0.95$—Full Flap: $\mu = 4.00$, $\sigma = 1.12$

6.2.5.3 Upwash Angle at Liftoff.

Figure 26 shows a plot of the estimated upwash angle as a function of the true airspeed and altitude above ground level. Curves for altitudes from 0 to 60 feet are shown, as well as a curve for the upwash calculated outside of ground effect. The upwash angle within ground effect is greatly affected by altitude. On the ground at 110 knots, the upwash angle is almost 1 degree smaller than the no ground effect case. Ground effect quickly diminishes and becomes negligible when the aircraft reaches an altitude above ground level greater than 50 feet. An aircraft weight of 17,000 lbf was used in the calculation of these angles because information on the actual aircraft weight at takeoff was not known.

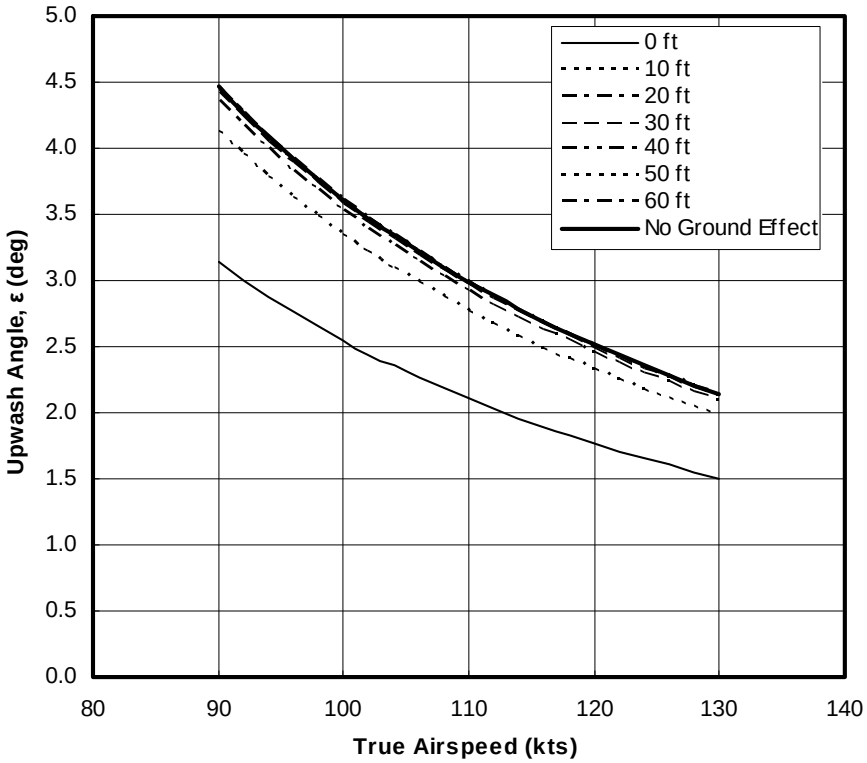

Figure 26. Wing Upwash Angle in Ground Effect—Aircraft Weight = 17,000 lbf

The combination of angle of attack, upwash angle, and engine nacelle tilt angle constitute the total inflow angle. Figure 27 shows the probability of the inflow angle at liftoff. The reader is cautioned that the values shown here do not include the nacelle tilt angle. Similar trends to those in figure 25 are observed in this figure, but the magnitudes of the angles have increased by about 2 degrees. The 2-degree shift represents the estimated upwash angle at liftoff. Again, the result for the no flaps case shown in figure 27 is unreliable due to the small sample size.

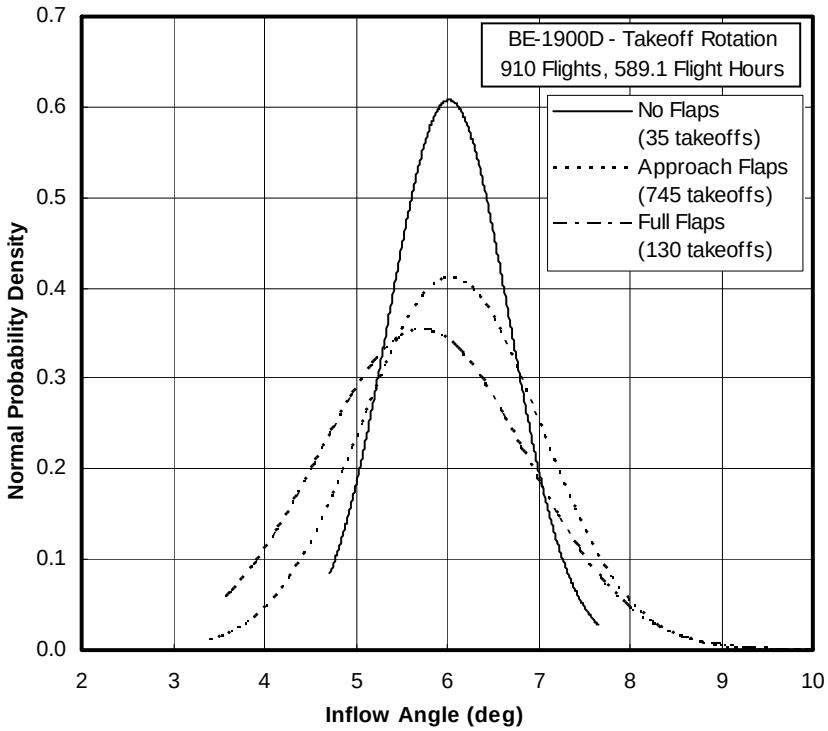

(a) Probability Density

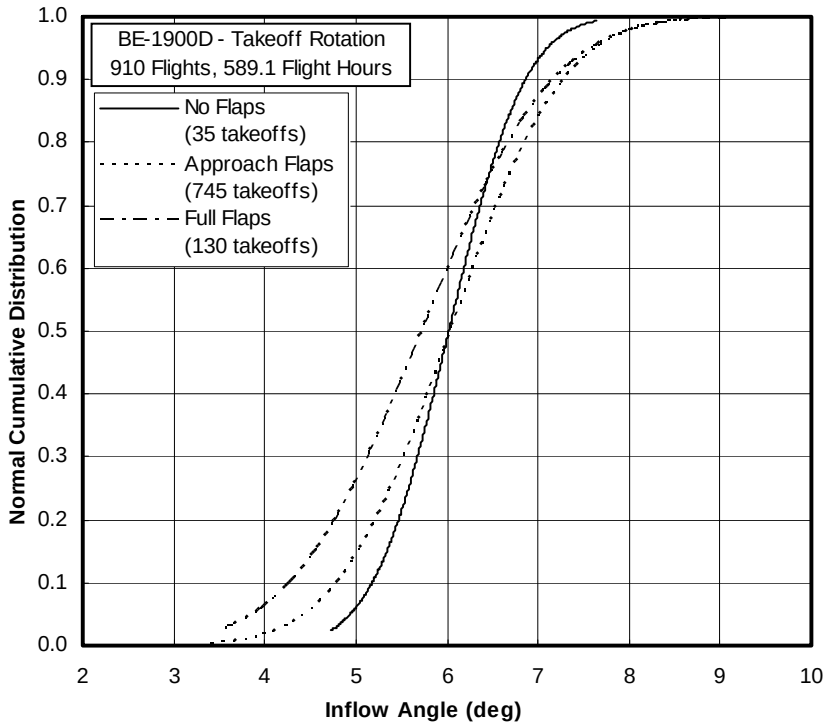

(b) Cumulative Distribution

Figure 27. Normal Probability of Inflow Angle Minus Nacelle Tilt Angle at Liftoff
No Flap: $\mu = 6.02$, $\sigma = 0.66$—Half Flap: $\mu = 6.04$, $\sigma = 0.97$—Full Flap: $\mu = 5.72$, $\sigma = 1.13$

The data presented in figures 25 and 27 shows the angle of attack and inflow angle at liftoff. The reader is reminded that liftoff was defined as the point of maximum angle of attack within 10 seconds after rotation. Thus, it is likely the aircraft was airborne at this point.

To quantify the ground effect upwash reduction, the probability distributions of the liftoff inflow angle with and without ground effect are shown in figure 28. The data in this figure pertains to cases where takeoff was performed with approach flaps and excludes the nacelle tilt angle. It is clear from this figure that ground effect decreased the upwash angle by about 0.55 degree, which could be significant considering the overall magnitudes.

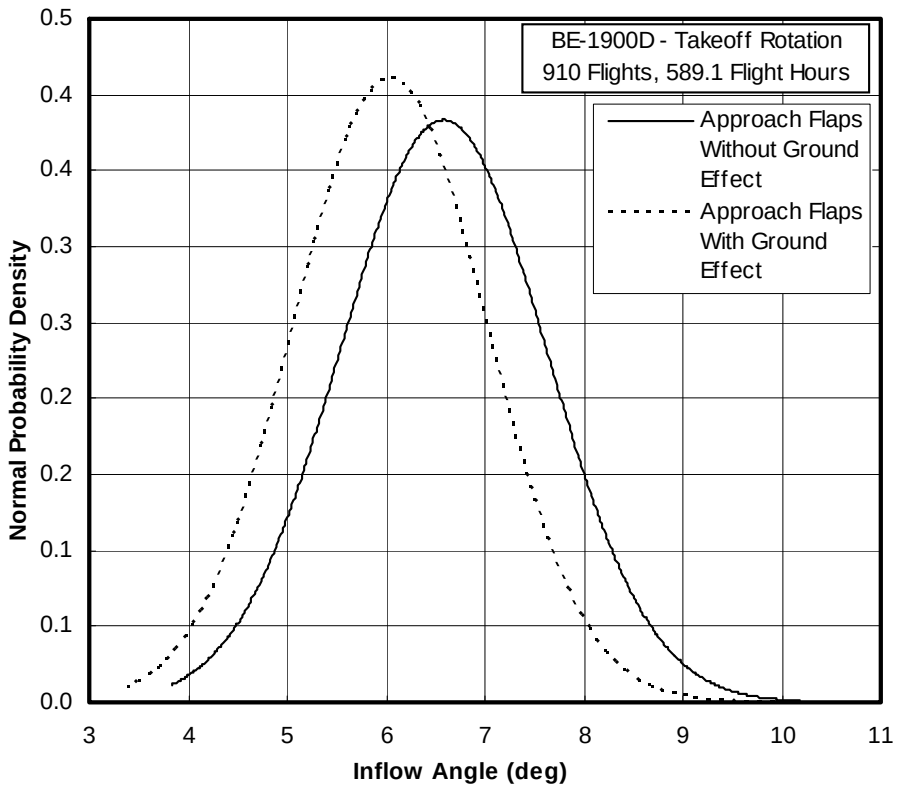

Figure 28. Ground Effect on Normal Probability of the Inflow Angle at Liftoff Minus Nacelle Tilt Angle, Ground Effect: $\mu = 6.04$, $\sigma = 0.97$—No Ground Effect: $\mu = 6.58$, $\sigma = 1.04$

6.3 FLIGHT OPERATIONS.

6.3.1 Aerodynamics Data.

6.3.1.1 Angle of Attack.

For each of the five flight phases, the occurrences of angle of attack were extracted and normalized to cumulative occurrences per 1000 hours and per nautical mile. The results are shown in figure 29. Again, each occurrence corresponded to 1 second of operation.

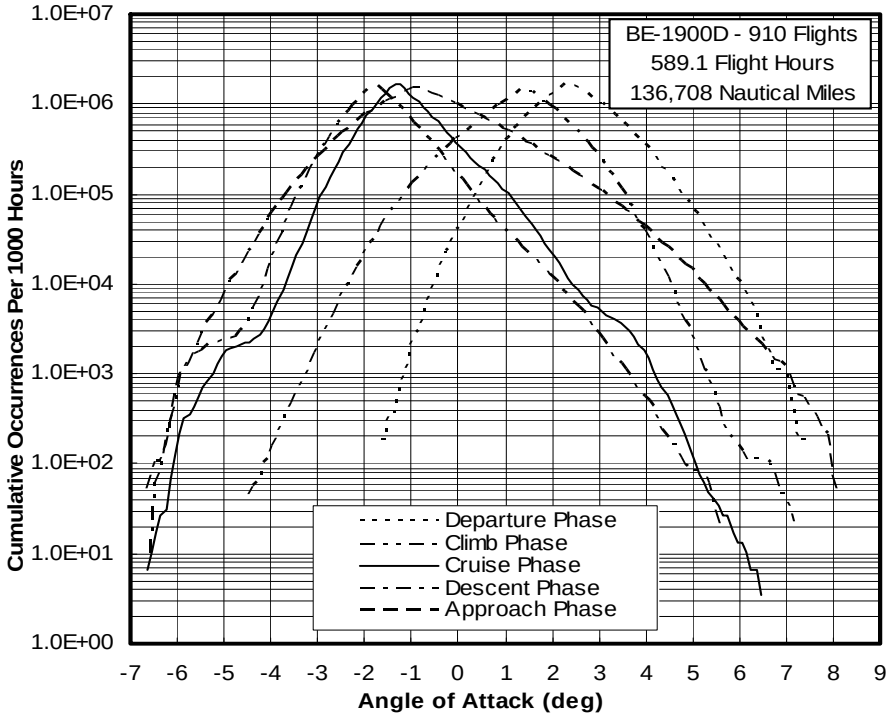

(a) Per 1000 Hours

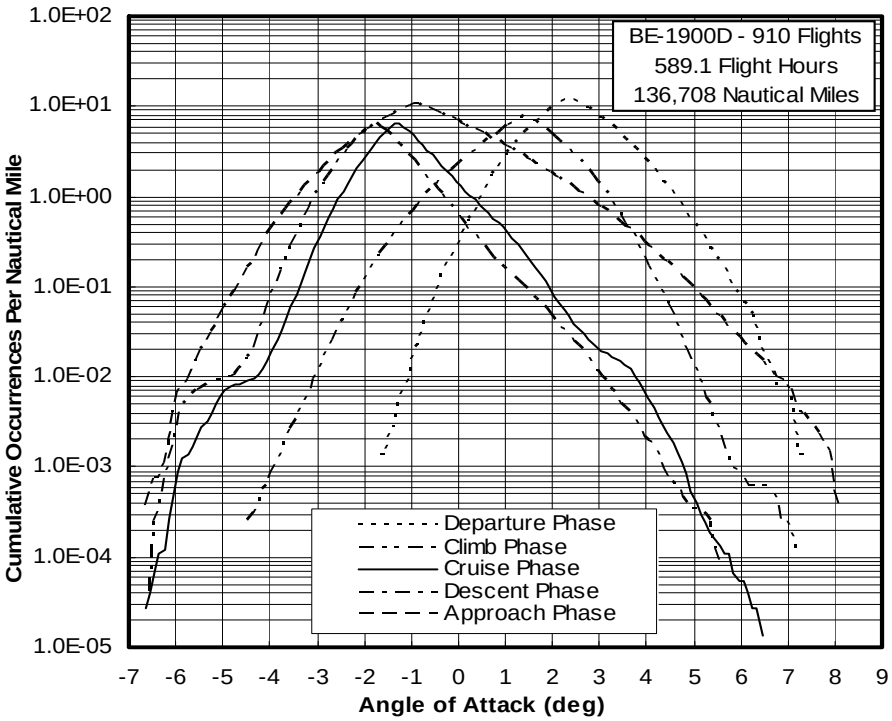

(b) Per Nautical Mile

Figure 29. Cumulative Occurrences of Angle of Attack During the Five Flight Phases

As expected, the departure phase of flight produced the highest angles of attack. Departure is a transitional phase from takeoff to climb, and consequently, the climbing airspeed is typically higher than during the departure segment. The lower airspeed results in higher angles of attack during departure compared to climb. The same is true for the airspeeds of cruise compared to climb—cruise airspeeds are significantly higher than climb airspeeds and accordingly, cruise angles of attack are considerably lower.

For descent, the angle of attack plot shows a trend very similar to the cruise phase with just a slightly lower mean. Airspeed increases by a small amount in descent from the cruise phase, and thus, there is a small decrease in the attack angles. The mean angle of attack during approach is slightly higher than cruise, but the angles span a wider range. This wide range can be explained by noting that approach serves as a transition phase between descent and landing, and thus, a somewhat large airspeed change takes place during this phase. This decrease in airspeed necessitates an increase in angle of attack. A change in flap position from approach to down could also have contributed to this wide range. Approach was identified by a flap deployment from the up position to either approach or down. If approach flaps were initially selected, a change in the angle of attack might occur upon the deployment of full flaps. Flaring before landing also results in a large increase in the angle of attack, and accordingly, added to the wide range of angles. Aircraft weight also influences the angle of attack, but since takeoff weight was not a known parameter, the data could not be categorized according to this parameter.

Data similar to that of figure 29 is presented in table 11(a) through (e). These tables show the angle of attack and coincident dynamic pressure for each of the flight phases, as percentages of total occurrence. Departure airspeed is lower than climb, resulting in higher angles of attack. The same is true for climb compared to cruise. The airspeed is slightly higher in descent than in cruise, which resulted in slightly lower angles of attack. In table 11(e), the transitional nature of the approach phase is clearly illustrated. The airspeeds during approach are lower than during climb, cruise, and descent, and also span a wider range than departure. The airplanes generally cruised within a dynamic pressure range of about 150 to 175 psf, descended at a slightly higher 175- to 200-psf range, and climbed at a low 75- to 100-psf range. Note that the angle of attack range for each flight phase table is unique.

The reader is reminded again that since data was collected at 1 Hz, each angle of attack occurrence corresponds to 1 second of flight operation. However, a comparison of the total occurrences given in table 11 with the information in figure 8 shows a discrepancy—the values given in table 11 are all less than what one would obtain from figure 8. This is a result of the angle of attack not being calculated when the aircraft banked more than 5 degrees. As a reminder, the method of determining the angle of attack was valid only for small bank angles.

Table 11. Percentage of Occurrence of Angle of Attack and Coincident Dynamic Pressure

(a) Departure (17,528 Total Occurrences)

Departure Phase		Dynamic Pressure, q (lb/ft²)										
		0-25	25-50	50-75	75-100	100-125	125-150	150-175	175-200	200-225	225-250	Total
Angle of Attack, α (deg)	-2.5 to -2	0	0	0	0	0	0	0	0	0	0	0
	-2 to -1.5	0	0	0	0.0057	0	0	0	0	0	0	0.0057
	-1.5 to -1	0	0	0.0171	0.0171	0	0	0	0	0	0	0.0342
	-1 to -0.5	0	0.0399	0.1198	0.0742	0	0	0	0	0	0	0.23
	-0.5 to 0	0	0.1198	0.4906	0.1883	0	0	0	0	0	0	0.80
	0 to 0.5	0	0.3994	1.4206	0.7588	0	0	0	0	0	0	2.58
	0.5 tot 1	0	1.1239	4.2161	1.489	0	0	0	0	0	0	6.83
	1 to 1.5	0	1.3864	8.3295	1.4605	0	0	0	0	0	0	11.18
	1.5 to 2	0	1.6146	12.785	1.3236	0	0	0	0	0	0	15.72
	2 to 2.5	0	1.9968	14.217	0.9471	0	0	0	0	0	0	17.16
	2.5 to 3	0	2.4703	12.454	0.3309	0	0	0	0	0	0	15.26
	3 to 3.5	0	2.2079	9.8699	0.0856	0	0	0	0	0	0	12.16
	3.5 to 4	0	2.1965	6.1958	0.0171	0	0	0	0	0	0	8.41
	4 to 4.5	0	1.9055	3.2805	0	0	0	0	0	0	0	5.19
	4.5 to 5	0	1.084	1.4662	0.0057	0	0	0	0	0	0	2.56
	5 to 5.5	0	0.5306	0.6219	0	0	0	0	0	0	0	1.15
	5.5 to 6	0	0.2853	0.1769	0	0	0	0	0	0	0	0.46
	6 to 6.5	0	0.1369	0.0685	0	0	0	0	0	0	0	0.21
	6.5 to 7	0	0.0342	0.0114	0	0	0	0	0	0	0	0.0456
	7 to 7.5	0	0.0114	0.0057	0	0	0	0	0	0	0	0.0171
	7.5 to 8	0	0.0057	0	0	0	0	0	0	0	0	0.0057
	8 to 8.5	0	0	0	0	0	0	0	0	0	0	0
	Total	0	17.55	75.75	6.70	0	0	0	0	0	0	100

(b) Climb (249,543 Total Occurrences)

Climb Phase		Dynamic Pressure, q (lb/ft²)										
		0-25	25-50	50-75	75-100	100-125	125-150	150-175	175-200	200-225	225-250	Total
Angle of Attack, α (deg)	-5 to -4.5	0	0	0	0	0	0	0	0	0	0	0
	-4.5 to -4	0	0	0	0	0	0	0.0012	0.0028	0	0	0.004
	-4 to -3.5	0	0	0	0.0012	0.0012	0.0068	0.0012	0.0024	0	0	0.013
	-3.5 to -3	0	0	0	0.0016	0.0152	0.0232	0.0028	0.0008	0	0	0.044
	-3 to -2.5	0	0	0.0004	0.004	0.0369	0.0685	0.0421	0.006	0	0	0.16
	-2.5 to -2	0	0	0.0012	0.0168	0.1238	0.2144	0.0874	0.0112	0.0028	0	0.46
	-2 to -1.5	0	0	0.002	0.0561	0.3599	0.561	0.1719	0.0108	0	0	1.16
	-1.5 to -1	0	0	0.004	0.2144	0.8528	0.775	0.2593	0.0353	0	0	2.14
	-1 to -0.5	0	0	0.018	0.7462	1.6442	1.191	0.4284	0.0457	0	0	4.07
	-0.5 to 0	0	0	0.0641	1.7656	2.5286	1.31	0.3482	0.0337	0.0012	0	6.05
	0 to 0.5	0	0	0.2096	4.1183	3.1578	0.9726	0.2661	0.0272	0	0	8.75
	0.5 tot 1	0	0	0.5358	8.7957	3.2455	0.5767	0.1362	0.0192	0	0	13.31
	1 to 1.5	0	0	0.9582	13.233	2.4918	0.4079	0.0721	0.0028	0	0	17.17
	1.5 to 2	0	0	1.4438	13.33	1.7083	0.1675	0.0345	0.0008	0	0	16.68
	2 to 2.5	0	0	1.954	10.336	0.8271	0.0701	0.008	0	0	0	13.19
	2.5 to 3	0	0.0012	2.3339	6.1208	0.2977	0.022	0.0048	0	0	0	8.78
	3 to 3.5	0	0.0004	1.8309	2.7983	0.0886	0.004	0	0	0	0	4.72
	3.5 to 4	0	0.002	1.0231	1.1697	0.0144	0.0004	0	0	0	0	2.21
	4 to 4.5	0	0.0004	0.4372	0.3438	0.0016	0	0	0	0	0	0.78
	4.5 to 5	0	0	0.1619	0.0613	0	0	0	0	0	0	0.22
	5 to 5.5	0	0	0.0485	0.0084	0	0	0	0	0	0	0.06
	5.5 to 6	0	0	0.0084	0.002	0	0	0	0	0	0	0.010
	6 to 6.5	0	0	0.0008	0	0	0	0	0	0	0	0.001
	6.5 to 7	0	0	0.002	0	0.0004	0.0004	0	0	0	0	0.003
	7 to 7.5	0	0	0.0012	0	0	0	0	0	0	0	0.001
	7.5 to 8	0	0	0	0	0	0	0	0	0	0	0
	Total	0	0.004	11.04	63.12	17.40	6.37	1.86	0.20	0.004	0	100

Table 11. Percentage of Occurrence of Angle of Attack and Coincident Dynamic Pressure (Continued)

(c) Cruise (964,870 Total Occurrences)

Cruise Phase		Dynamic Pressure, q (lb/ft²)										
		0-25	25-50	50-75	75-100	100-125	125-150	150-175	175-200	200-225	225-250	Total
Angle of Attack, α (deg)	-6.5 to -6	0	0	0	0.0006	0	0	0.0028	0	0	0	0.003
	-6 to -5.5	0	0	0	0.0003	0	0.0019	0.0107	0	0	0	0.013
	-5.5 to -5	0	0	0	0.0005	0.0001	0.0131	0.0179	0	0	0	0.032
	-5 to -4.5	0	0	0.0002	0.0006	0.0006	0.0055	0.0103	0.0012	0	0	0.018
	-4.5 to -4	0	0	0.0005	0.003	0.0015	0.0048	0.0197	0.0206	0	0	0.050
	-4 to -3.5	0	0	0.0001	0.0061	0.0038	0.038	0.1969	0.1023	0.0003	0	0.35
	-3.5 to -3	0	0	0.0011	0.0175	0.0137	0.1233	1.1528	0.3385	0.0027	0	1.65
	-3 to -2.5	0	0	0.0027	0.0302	0.0447	0.2952	3.4163	1.1608	0.0047	0	4.95
	-2.5 to -2	0	0	0.0035	0.0465	0.1276	1.2459	7.9789	2.5971	0.0066	0	12.01
	-2 to -1.5	0	0	0.0055	0.0511	0.2643	2.9094	14.078	3.951	0.0231	0	21.28
	-1.5 to -1	0	0	0.0081	0.0738	0.5931	5.0084	14.088	3.6133	0.0257	0	23.41
	-1 to -0.5	0	0	0.0086	0.1203	0.984	5.5025	8.6463	1.4854	0.0087	0	16.76
	-0.5 to 0	0	0	0.0107	0.2144	1.4969	3.3121	3.9631	0.4441	0.0044	0	9.45
	0 to 0.5	0	0.0001	0.0106	0.3194	1.1285	1.4739	1.3835	0.1078	0.0002	0	4.42
	0.5 tot 1	0	0.0005	0.0141	0.4379	0.7133	0.6841	0.6373	0.0339	0	0	2.52
	1 to 1.5	0	0.0005	0.0177	0.5775	0.3902	0.4152	0.233	0.0042	0	0	1.64
	1.5 to 2	0	0.0016	0.0324	0.4404	0.2005	0.116	0.0483	0.0007	0	0	0.84
	2 to 2.5	0	0.002	0.041	0.2033	0.0665	0.0245	0.0091	0	0	0	0.35
	2.5 to 3	0	0.0002	0.0298	0.0636	0.0129	0.0048	0.0015	0	0	0	0.11
	3 to 3.5	0	0	0.0256	0.0188	0.0017	0.0022	0	0	0	0	0.048
	3.5 to 4	0	0	0.0519	0.0047	0.0002	0.0001	0	0.0001	0	0	0.057
	4 to 4.5	0	0	0.0297	0.0013	0.0001	0	0	0.0001	0	0	0.031
	4.5 to 5	0	0	0.0111	0	0	0	0	0	0	0	0.011
	5 to 5.5	0	0	0.0021	0	0	0	0	0	0	0	0.002
	Total	0	0.005	0.31	2.63	6.04	21.18	55.89	13.86	0.076	0	100

(d) Descent (294,140 Total Occurrences)

Descent Phase		Dynamic Pressure, q (lb/ft²)										
		0-25	25-50	50-75	75-100	100-125	125-150	150-175	175-200	200-225	225-250	Total
Angle of Attack, α (deg)	-6.5 to -6	0	0	0	0	0	0	0	0.0139	0	0	0.014
	-6 to -5.5	0	0	0	0	0.0007	0	0.0007	0.0401	0	0	0.041
	-5.5 to -5	0	0	0	0	0.0014	0.001	0.0037	0.0122	0	0	0.018
	-5 to -4.5	0	0	0	0.0017	0.0041	0.0037	0.0095	0.015	0.001	0	0.035
	-4.5 to -4	0	0	0	0.0092	0.0112	0.0173	0.0986	0.2128	0.0184	0	0.37
	-4 to -3.5	0	0	0.0003	0.0214	0.0306	0.1217	0.4447	1.1478	0.0697	0	1.84
	-3.5 to -3	0	0	0.0034	0.0374	0.1044	0.2628	1.3446	3.3358	0.4008	0	5.49
	-3 to -2.5	0	0	0.0133	0.0483	0.2166	0.7238	2.7949	7.3652	0.6803	0	11.84
	-2.5 to -2	0	0	0.0235	0.0972	0.4783	1.4901	5.1333	11.558	0.9846	0	19.77
	-2 to -1.5	0	0	0.036	0.1326	0.7809	2.32	7.0596	11.648	0.9924	0	22.97
	-1.5 to -1	0	0.0003	0.0619	0.1516	1.145	2.7382	5.306	7.6729	0.5929	0	17.67
	-1 to -0.5	0	0.0003	0.0949	0.2047	1.6873	2.1877	2.6161	3.0999	0.2822	0	10.17
	-0.5 to 0	0	0	0.1363	0.2856	1.3579	1.1138	1.0716	1.1107	0.083	0	5.16
	0 to 0.5	0	0.0014	0.136	0.375	0.7207	0.4318	0.3781	0.3223	0.0337	0	2.40
	0.5 tot 1	0	0.0024	0.1234	0.2713	0.3301	0.154	0.0881	0.0598	0.0065	0	1.04
	1 to 1.5	0	0.0024	0.0901	0.2451	0.1336	0.0313	0.0116	0.0031	0.0014	0	0.52
	1.5 to 2	0	0.0007	0.0615	0.1278	0.1176	0.0095	0.0024	0.0003	0.0014	0	0.32
	2 to 2.5	0	0	0.0394	0.0768	0.0513	0.0007	0	0	0	0	0.17
	2.5 to 3	0	0	0.0405	0.0425	0.0167	0	0	0	0	0	0.10
	3 to 3.5	0	0	0.0204	0.019	0.0037	0	0	0	0	0	0.043
	3.5 to 4	0	0	0.0105	0.0078	0.001	0	0.0003	0.0003	0	0	0.020
	4 to 4.5	0	0	0.0102	0.0003	0.0003	0	0	0	0	0	0.011
	4.5 to 5	0	0	0.0024	0	0	0	0	0	0	0	0.0024
	5 to 5.5	0	0	0.002	0	0	0	0	0	0	0	0.002
	Total	0	0.007	0.91	2.16	7.19	11.61	26.36	47.62	4.15	0	100

Table 11. Percentage of Occurrence of Angle of Attack and Coincident Dynamic Pressure (Continued)

(e) Approach (113,418 Total Occurrences)

Approach Phase		Dynamic Pressure, q (lb/ft²)										
		0-25	25-50	50-75	75-100	100-125	125-150	150-175	175-200	200-225	225-250	Total
Angle of Attack, α (deg)	-6 to -5.5	0	0.0018	0.0185	0.0159	0.0185	0	0	0	0	0	0.055
	-5.5 to -5	0	0.0026	0.0538	0.0555	0.0432	0	0	0	0	0	0.16
	-5 to -4.5	0	0.0035	0.1772	0.1384	0.0899	0	0	0	0	0	0.41
	-4.5 to -4	0.0009	0.0115	0.4259	0.4444	0.2654	0	0	0	0	0	1.15
	-4 to -3.5	0	0.0335	0.932	0.9769	0.3333	0	0	0	0	0	2.28
	-3.5 to -3	0.0106	0.0908	1.6549	1.6347	0.432	0	0	0	0	0	3.82
	-3 to -2.5	0.0317	0.2777	2.8435	2.7826	0.6533	0	0	0	0	0	6.59
	-2.5 to -2	0.0432	0.5281	4.0302	4.0152	0.6807	0	0	0	0	0	9.30
	-2 to -1.5	0.0547	0.8447	5.6217	4.3468	0.5361	0	0	0	0	0	11.40
	-1.5 to -1	0.0529	1.3366	6.5633	3.8742	0.3024	0	0	0	0	0	12.13
	-1 to -0.5	0.0732	1.5782	7.1699	2.6248	0.1525	0.0035	0	0	0	0	11.60
	-0.5 to 0	0.0414	1.7369	6.5298	1.4354	0.0829	0.0026	0	0	0	0	9.83
	0 to 0.5	0.0476	1.617	5.5185	0.8164	0.045	0	0	0	0	0	8.04
	0.5 tot 1	0.03	1.5826	4.3917	0.4038	0.0185	0.0009	0	0	0	0	6.43
	1 to 1.5	0.0247	1.6382	3.19	0.2389	0.0097	0	0	0	0	0	5.10
	1.5 to 2	0.015	1.4724	2.027	0.1146	0.0009	0	0	0	0	0	3.63
	2 to 2.5	0.0115	1.4416	1.1638	0.0441	0	0	0	0	0	0	2.66
	2.5 to 3	0.0097	1.2353	0.6145	0.0388	0	0	0	0	0	0	1.90
	3 to 3.5	0.0053	0.9857	0.276	0.0265	0	0	0	0	0	0	1.29
	3.5 to 4	0.0053	0.7406	0.1437	0.0044	0	0	0	0	0	0	0.89
	4 to 4.5	0.0018	0.5176	0.0397	0.0009	0	0	0	0	0	0	0.56
	4.5 to 5	0.0035	0.3342	0.0141	0	0	0	0	0	0	0	0.35
	5 to 5.5	0.0009	0.201	0.0035	0	0	0	0	0	0	0	0.21
	5.5 to 6	0	0.1084	0.0009	0	0	0	0	0	0	0	0.11
	6 to 6.5	0	0.0467	0	0	0	0	0	0	0	0	0.047
	6.5 to 7	0	0.0256	0	0	0	0	0	0	0	0	0.026
	7 to 7.5	0	0.0229	0	0	0	0	0	0	0	0	0.023
	7.5 to 8	0	0.0097	0.0018	0	0	0	0	0	0	0	0.011
	Total	0.46	18.43	53.41	24.03	3.66	0.007	0	0	0	0	100

6.3.1.2 Upwash Angle.

To extract the total inflow angle experienced during each segment of flight from table 11, the upwash angle must be known. Figure 30 presents a plot of the calculated upwash angle as a function of the dynamic pressure for various aircraft weights. Departure dynamic pressures of between 25 to 50 psf produced the highest upwash angles that were between 2 and 4 degrees. This angle decreased quickly and was less than 1.5 degrees at climb dynamic pressures and about 0.5 degree during cruise. The effect of aircraft weight was much more pronounced at lower dynamic pressures. Using information from this figure and table 11, the departure that produced the largest inflow angles can be shown. Coupled with a higher takeoff weight and higher power settings, the propeller blades would experience the largest 1P loads during this phase. Figure 30 does not include ground effect and should not be used for extracting the upwash angle at takeoff rotation.

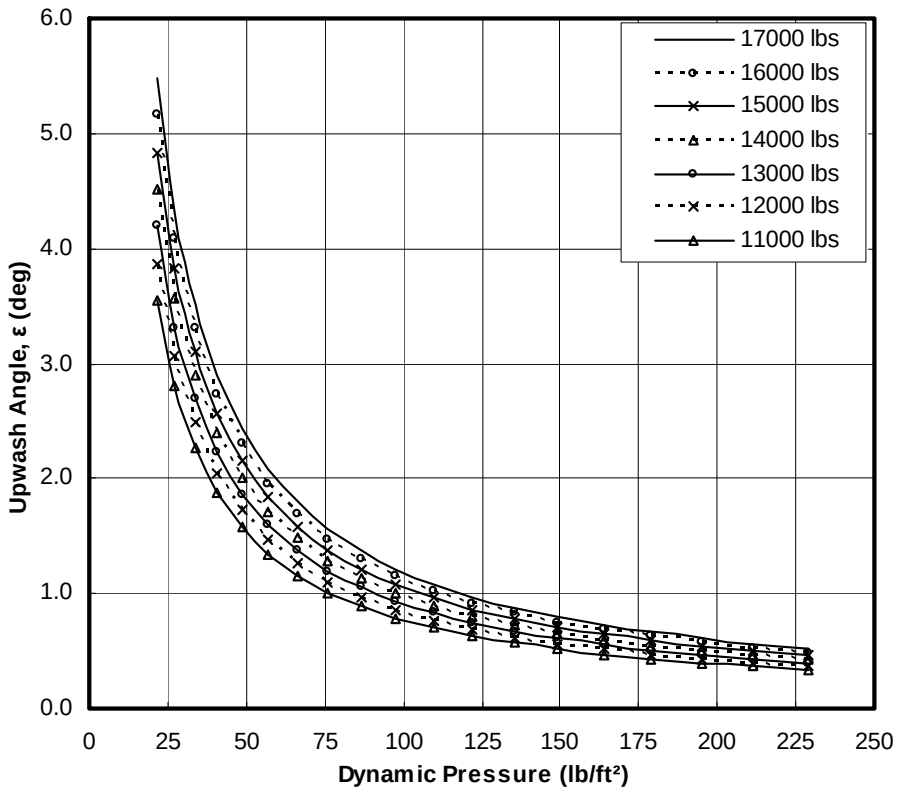

Figure 30. Upwash Angle as a Function of Dynamic Pressure for Various Aircraft Weights

6.3.2 In-Flight Engine and Propeller Usage.

The correlation of the engine torque and propeller shaft speed, as shown in table 12, shows how the engines and propellers were used in flight. This table shows the propellers spent the majority of flight time at speeds of 1450 to 1500 rpm and the engines at torque levels between 3000 and 3600 ft-lbf. A typical cruise power setting, as observed in the data files, was a propeller shaft speed of just below 1500 rpm and a torque that varied between 3000 and 3600 ft-lbf, depending on the pressure altitude. The shaft speed during climb was just below 1600 rpm, and thus the smaller peak in percentages for the range between 1550 and 1600 rpm. High torque applied to low shaft speeds was of interest, as well as the frequency of its occurrence. As shown in table 12, this did not happen often. A torque of more than 3400 ft-lbf was applied very rarely at shaft speeds less than 1450 rpm. The small percentages of flights with shaft speeds, below 1100 were most likely due to the method used for identifying a flight by airspeed alone. During a landing, the aircraft touches down at airspeeds greater than 84 knots with the power set to idle, and thus, the propeller shaft speed might decrease to these low values.

Table 13 presents data very similar to that in table 12 but correlates the thrust with the shaft speed. Thrust was extracted from the propeller performance maps provided by Hartzell Propeller, Inc. Thrust could not be obtained for all flight conditions. In some situations, the power coefficient, the advance ratio, or the propeller tip Mach number was outside the range of the performance maps. This is the reason for the disparity in the percentage of occurrence of the shaft speeds between tables 12 and 13. However, table 13 shows the same trend in the percentage of operation at different shaft speeds as table 12.

Table 12. Correlation of Engine Torque and Propeller Shaft Speed as a Percentage of Flight Time

BE-1900D	RPM/100																	
910 Flights	< 10	10-10.5	10.5-11	11-11.5	11.5-12	12-12.5	12.5-13	13-13.5	13.5-14	14-14.5	14.5-15	15-15.5	15.5-16	16-16.5	16.5-17	17-17.5	17.5-18	Total
Torque (ft-lbf/100)																		
0-2	0.0001	7E-05	0.0004	0.0015	0.0057	0.0184	0.0358	0.0524	0.0573	0.0692	0.2216	0.0729	0.1229	0.0249	0.0004	0.0052	0	0.69
2-4	0.0009	0.0008	0.0012	0.0027	0.0047	0.0069	0.0085	0.0088	0.0087	0.0164	0.2185	0.0496	0.1685	0.0411	7E-05	0.0022	0	0.54
4-6	0.0012	0.0004	0.0005	0.0005	0.0004	0.0005	0.0007	0.001	0.0023	0.0234	0.3868	0.0702	0.2963	0.0623	2E-05	7E-05	2E-05	0.85
6-8	0.0004	0.0002	0.0002	0.0002	0.0001	0.0002	0.0002	0.0006	0.0011	0.0199	0.5046	0.1067	0.6758	0.1552	5E-05	0.0001	0	1.47
8-10	0.0006	0.0001	0.0002	0.0001	0.0002	0.0003	9E-05	0.0003	0.0008	0.0356	0.8329	0.2178	1.1121	0.2295	0.0002	0.0004	0	2.43
10-12	0.0004	0.0002	5E-05	9E-05	5E-05	9E-05	7E-05	0.0001	0.0009	0.0427	0.9293	0.1673	0.6284	0.1365	0.0001	0.0002	0	1.91
12-14	0.0002	7E-05	2E-05	7E-05	5E-05	5E-05	2E-05	2E-05	0.0004	0.0833	1.0088	0.1962	0.224	0.0477	2E-05	0	0	1.56
14-16	2E-05	0	7E-05	0	2E-05	0.0001	0.0006	0.0009	0.0013	0.0677	1.3009	0.2476	0.1228	0.0371	0.0005	0.0007	0.0041	1.78
16-18	0	2E-05	0.0002	0.001	0.0027	0.0051	0.0077	0.0098	0.0094	0.11	1.6296	0.2456	0.0808	0.0349	0.0005	0.0054	0.0085	2.15
18-20	0.0002	0.0003	0.0004	0.0002	0.0002	0.0002	0.0002	0.0003	0.0033	0.087	1.5217	0.2623	0.0752	0.0547	0.0004	0.0154	0.0332	2.06
20-22	0.0002	7E-05	2E-05	5E-05	5E-05	0	0	0	0.003	0.0875	1.4029	0.2626	0.0816	0.0543	0.0007	0.0155	0.031	1.94
22-24	5E-05	5E-05	2E-05	5E-05	5E-05	0	2E-05	2E-05	0.0012	0.1189	1.7906	0.3775	0.2218	0.1133	0.0001	0.0141	0.0224	2.66
24-26	5E-05	5E-05	5E-05	0	5E-05	0	0	0	0.001	0.1393	2.9277	0.4757	0.2566	0.1922	0.0004	0.0134	0.0203	4.03
26-28	2E-05	0	0	2E-05	2E-05	0	0	0	0.0006	0.1878	3.096	0.4417	0.2808	0.3384	0.0022	0.0114	0.019	4.38
28-30	0	0	0	0	0	0	0	2E-05	0.004	0.4177	6.6936	0.807	0.98	0.9075	0.0084	0.0247	0.0137	9.86
30-32	0	0	0	0	0	0	0	0	0.0065	0.5995	9.7879	1.3505	2.0891	1.8896	0.0264	0.1119	0.0188	15.88
32-34	0	0	0	0	0	0	0	0	0.013	0.7518	10.823	1.4321	3.1884	2.3862	0.0515	0.2729	0.0324	18.95
34-36	0	0	0	0	0	0	0	0	0.0245	1.1538	13.544	2.5905	2.8466	1.7475	0.06	0.4122	0.0557	22.43
36-37.5	0	0	0	0	0	0	0	0	0.0081	0.244	2.0707	0.8893	0.5214	0.2042	0.0305	0.2395	0.0266	4.23
> 37.5	0	0	0	0	0	0	0	0	9E-05	0.0057	0.0346	0.0255	0.0279	0.0202	0.0102	0.0797	0.0048	0.209
Total	0.0044	0.0024	0.0033	0.007	0.014	0.032	0.054	0.074	0.15	4.26	60.73	10.29	14.00	8.68	0.19	1.23	0.29	100

Table 13. Correlation of Thrust and Propeller Shaft Speed as a Percentage of Flight Time

BE-1900D	RPM/100																	
910 Flights	< 10	10-10.5	10.5-11	11-11.5	11.5-12	12-12.5	12.5-13	13-13.5	13.5-14	14-14.5	14.5-15	15-15.5	15.5-16	16-16.5	16.5-17	17-17.5	17.5-18	Total
Thrust (lbf/100)																		
0-2	0.0074	0.0035	0.0045	0.0087	0.0179	0.0367	0.06	0.08	0.0958	0.5918	3.7945	0.4522	0.9477	0.182	0.0007	0.0074	2E-05	6.29
2-4	0	0	0	0	0	0	0	0	0.0004	0.0288	1.1156	0.3022	0.7372	0.1493	0.0001	9E-05	0	2.33
4-6	0	0	0	0	0	0	0	2E-05	0.0015	0.1389	2.2061	0.4972	1.4626	0.2888	0.0002	0.0004	0	4.60
6-8	0	0	0	0	0	0	0	0	0.0031	0.3386	6.2763	1.0377	0.6594	0.1577	0.0007	5E-05	0	8.47
8-10	0	0	0	0	0	0	0	0	0.0187	1.6607	21.729	2.6403	0.3818	0.2344	0.0001	0.0003	0.0079	26.67
10-12	0	0	0	0	0	0	0	0	0.0512	1.2891	25.75	4.8295	1.5046	1.4194	0.0015	0.0007	0.0111	34.86
12-14	0	0	0	0	0	0	0	0	0.0003	0.0214	0.4759	0.1975	2.3075	2.42	0.005	0.0023	0.0218	5.45
14-16	0	0	0	0	0	0	0	0	0	0.0003	0.0131	0.0796	3.1535	2.2766	0.0099	0.0063	0.0051	5.54
16-18	0	0	0	0	0	0	0	0	0	0	0.0002	0.0675	2.3182	1.3475	0.0217	0.0232	0.0116	3.79
18-20	0	0	0	0	0	0	0	0	0	0	7E-05	0.0047	0.3484	0.2393	0.0543	0.152	0.0177	0.82
20-22	0	0	0	0	0	0	0	0	0	0	2E-05	2E-05	0.0193	0.0214	0.0421	0.353	0.0353	0.47
22-24	0	0	0	0	0	0	0	0	0	0	0	0	0.0018	0.0007	0.0216	0.2666	0.0312	0.32
24-26	0	0	0	0	0	0	0	0	0	0	0	0	0.0006	0.0001	0.0158	0.171	0.0174	0.20
26-28	0	0	0	0	0	0	0	0	0	0	0	0	0.0003	0	0.0112	0.108	0.0106	0.13
28-30	0	0	0	0	0	0	0	0	0	0	0	0	9E-05	0	0.0027	0.0373	0.0045	0.045
30-32	0	0	0	0	0	0	0	0	0	0	0	0	0	0	0	0.0014	0.0003	0.0017
32-34	0	0	0	0	0	0	0	0	0	0	0	0	0	0	0	0.0003	0	0.0003
> 34	0	0	0	0	0	0	0	0	0	0	0	0	0	0	0	0	0	0
Total	0.0074	0.0035	0.0045	0.0087	0.0179	0.0367	0.06	0.0801	0.17	4.07	61.36	10.11	13.84	8.74	0.19	1.13	0.17	100

During the majority of the total flight time, thrust was in the 800- to 1200-lbf range. A small percentage of operation between 0 and 200 lbf of thrust is also shown. Similar to the torque data in table 12, a distinction between the flight phases cannot be made from the thrust percentages.

6.3.3 Effect of Gusts on Angle of Attack.

This section presents the results of the derived gust velocity data extracted from normal accelerations and its effect on instantaneous angle of attack. Derived gust velocities were converted into changes in the propeller inflow angle and are presented here as the cumulative occurrences per 1000 hours and per nautical mile. The reader is reminded that each occurrence had a duration of 1 second. The data was separated by flight phase and divided into various altitude bands indicated in figures 31-33.

Figure 31 shows the cumulative occurrences of the change in inflow angle during the climb phase of flight. The decrease in the level of turbulence with increasing altitude, and its effect on the angle of attack, is shown in this figure. The altitude band between 0 and 500 ft did not follow this trend exactly. This is likely due to the very short total time spent within this range, resulting in a small number of samples, and therefore, larger scatter in the normalized data. It is important to note that the data presented here pertains to gusts only and was extracted according to the 2-second rule. Despite the fact that this is a standard method of separating gusts and maneuvers, its validity can be legitimately questioned. This may be one reason for the data showing a larger number of occurrences of positive loads than negative loads in figure 31.

Figure 32 presents the same data for the cruise phase. Again, similar trends to those in figure 31 can be observed. The 501- to 1500-ft altitude band in this figure also did not follow the exact same pattern as the other altitude bands. This is again due to a very small amount of cruise time spent in this altitude band. Similar to the climb phase, an increase in inflow angle also showed a greater frequency of occurrence than a decrease in the angle. For a specific altitude band, the number of occurrences during cruise was about an order of magnitude smaller than during the climb phase. This is a direct result of the difference in airspeed between the two phases. For example, a derived gust velocity of 10 feet per second occurring while climbing at 170 knots would cause a change in inflow angle of about 2 degrees. The same gust speed while cruising at 220 knots would result in a change in inflow angle of 1.5 degrees.

Cumulative occurrences of change in angle of attack due to vertical gusts for the descent phases are shown in figure 33. In this case, the frequency of occurrence within similar altitude bands was comparable to the cruise phase. This is due to the similar airspeeds during these two phases. The traits observed in figure 33 showed no significant discrepancies with those observed in the previous figures.

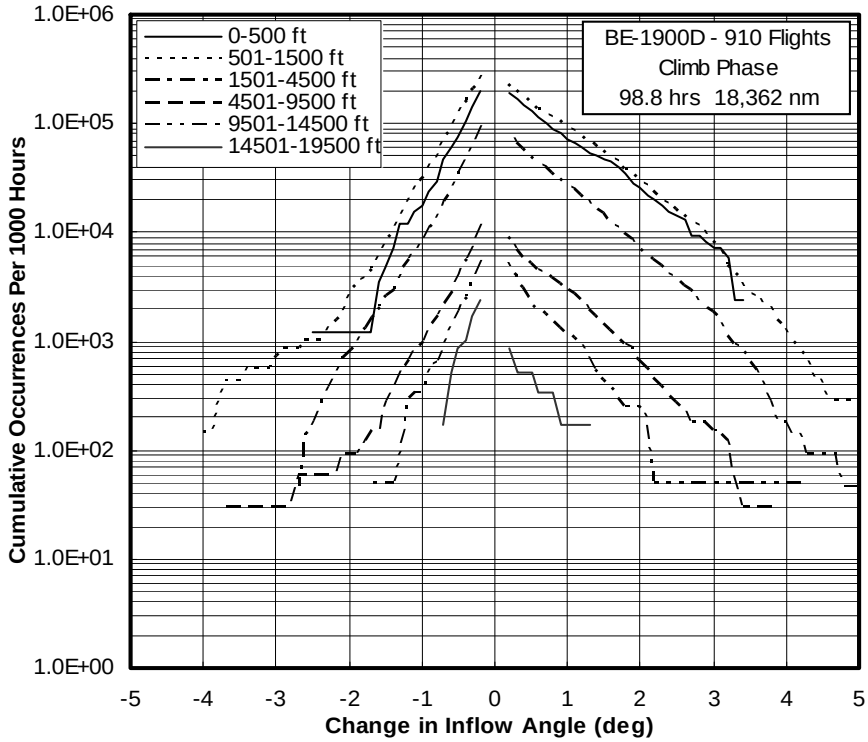

(a) Per 1000 Hours

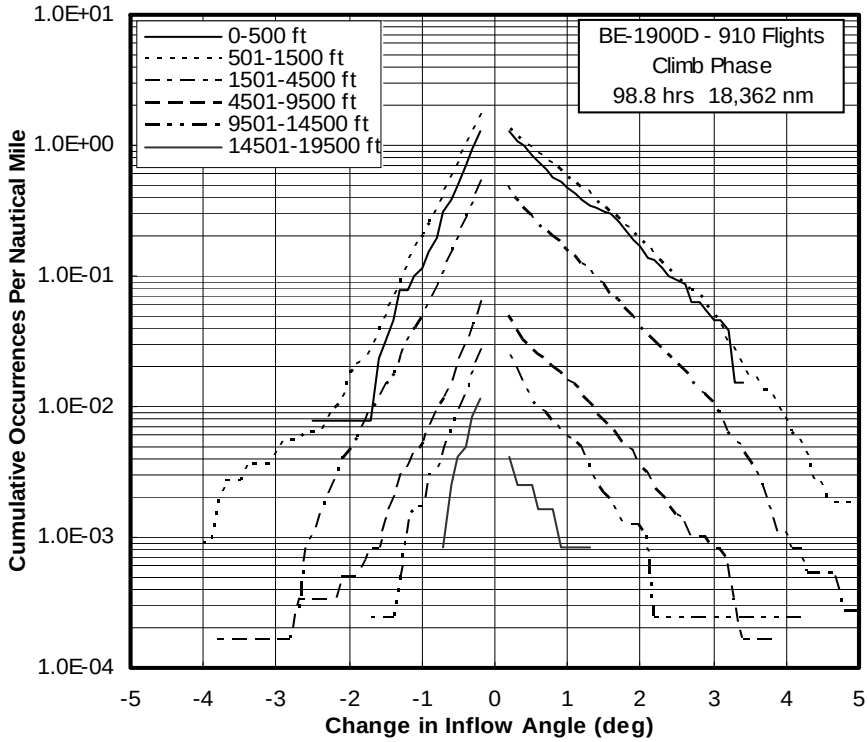

(b) Per Nautical Mile

Figure 31. Cumulative Occurrence $\Delta\alpha$ due to Gusts During Climb

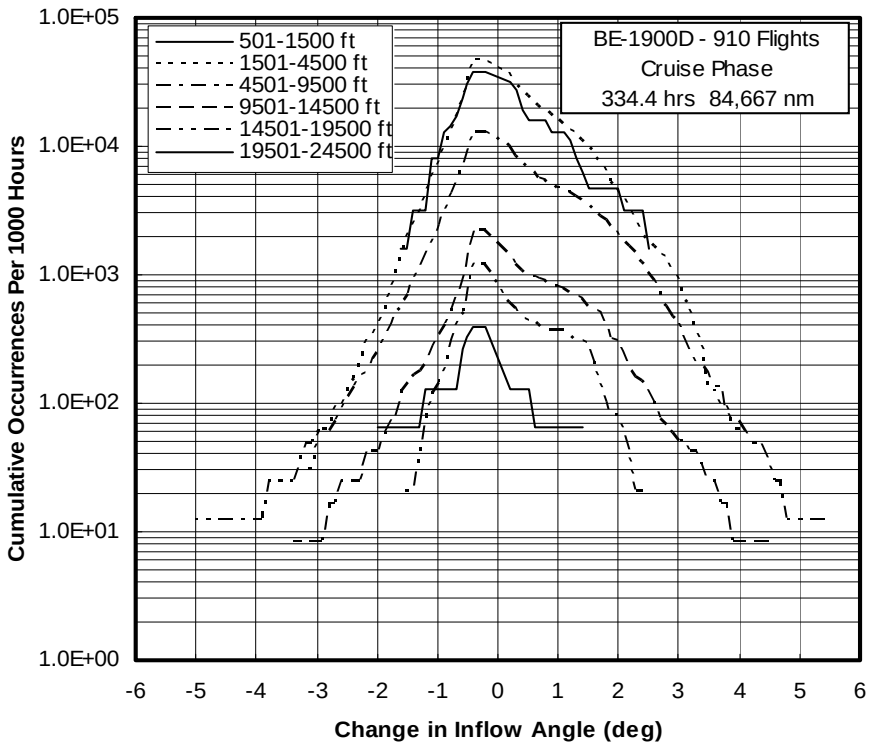

(a) Per 1000 Hours

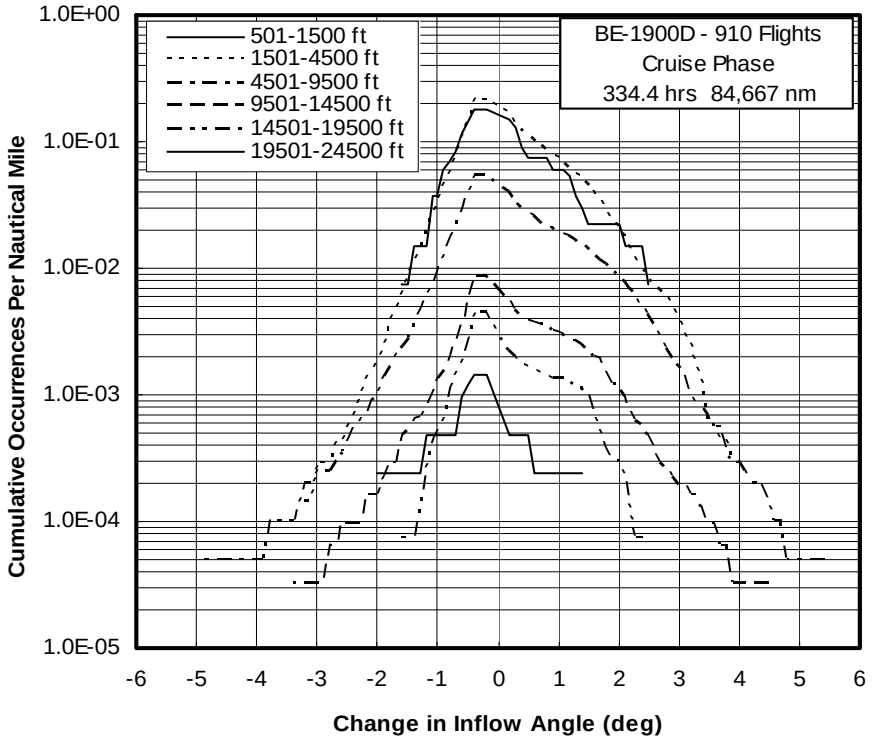

(b) Per Nautical Mile

Figure 32. Cumulative Occurrence $\Delta\alpha$ due to Gusts During Cruise

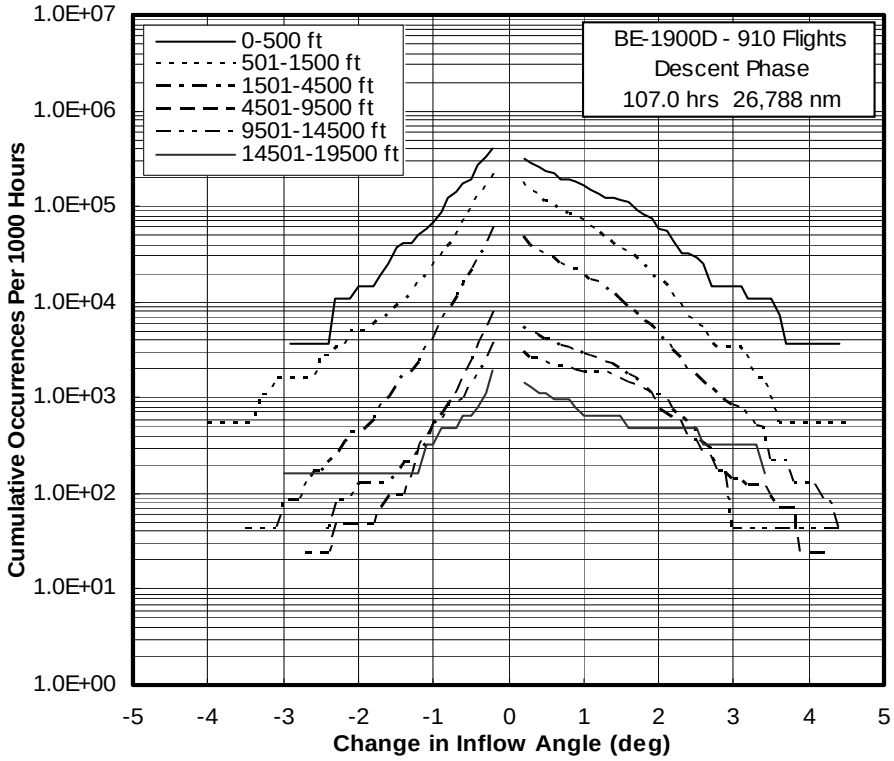

(a) Per 1000 Hours

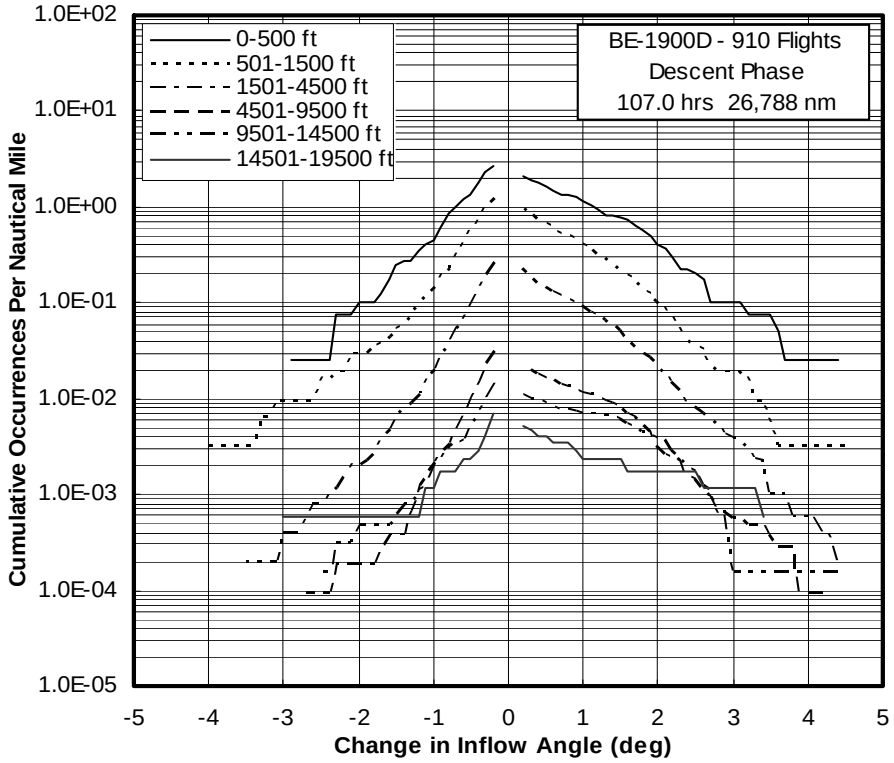

(b) Per Nautical Mile

Figure 33. Cumulative Occurrence $\Delta\alpha$ due to Gusts During Descent

7. CONCLUSIONS.

The objectives of this program were met. The overall quality of the data was quite good with 910 flights available to obtain reasonable statistical data, particularly considering that the data was not taken in a controlled laboratory setting.

The statistical data formats allowed a very in-depth examination of various parameters that influence the operation of the propellers on BE-1900D Beechcraft. The results presented here should be useful to the Federal Aviation Administration, the propeller manufacturer, and the airlines in gaining a better understanding of how these systems are used. In the following paragraphs, brief discussions of some of the noteworthy findings are presented.

The processed data presented in this report appears to match the expected outcomes, with a few small exceptions. For instance, the altitude, airspeed, and flight distance data revealed flight profiles that were consistent with a commuter-type aircraft. Flap usage was consistent with that expected on a commuter-aircraft. Some specific observations made are as follows.

- During ground operations, the right engine was used more often than the left engine.

- Ground operations of the propellers within the lower restricted revolutions per minute (rpm) range for more than 30 seconds accounted for about 10% of the total time on the ground. This is a significant amount of time within a prohibited propeller shaft speed range. Transitioning time through the restricted shaft speed ranges showed nothing out of the ordinary.

- Reverse propeller usage was more frequent during ground operations than during the landing rollout. Simultaneous propeller reversals occurred on only 320 of the 910 landings, accounting for about 38% of the total number of reversals.

- The data files indicated minor mismatch between the start times of the left and right propeller reversals during the landing rollout. It is unclear if this was caused by the positioning of the sensors or if it indicated actual asynchronous reversal of the two propellers. There are anecdotal references to the latter among pilots familiar with BE-1900D.

- Takeoff rotation was identified as the most severe phase of flight in terms of magnitude of the periodic loads on the propeller blades. Rotation airspeed averaged around 112 knots indicated airspeed, and the torque and shaft speed parameters indicated the engines were generally at full power for takeoff. A greater flap deflection was accompanied by a smaller angle of attack. Due to a small sample size for takeoffs without flaps, the results for this case were deemed unreliable. Angle of attack at liftoff for the most common case (approach flaps) was about 4.2 degrees, and the full flap takeoffs averaged about 4 degrees.

- Estimated upwash angle was shown to have significant influence on the inflow angle at the plane of the propeller, especially at low dynamic pressures and high gross weights.

The upwash angle at liftoff, which included the ground effect, was estimated to be about 2 degrees. The reduction in the upwash angle due to ground effect was estimated to be about 0.55 degree. High power settings coupled with high angles of attack and high upwash angles at liftoff were believed to lead to the highest vibratory loads on the propeller blades.

- Angle of attack for nonmaneuvering flight was shown to vary from -6 to +8 degrees, depending on the flight phase. Cumulative occurrences of this parameter for various flight phases were presented per nautical mile and per 1000 hours of operation. Departure produced the highest angles and descent the lowest, while approach indicated a wide spread of angles.

- Correlations of torque and thrust with the propeller shaft speed were also presented and proved to show no unusual traits. High engine torques applied to low shaft speeds were also considered. Torque levels greater than 3600 ft-lbf were very rarely applied at shaft speeds below 1450 rpm; the typical cruising shaft speed was between 1450 and 1500 rpm.

- Vertical gust speeds were extracted from the normal accelerations data and converted to the change in propeller inflow angle. This data was also presented as cumulative occurrences per nautical mile and per 1000 hours. A trend of decreasing occurrences and magnitude with increasing altitude was observed. Increased airspeed was also shown to decrease the severity of the effect on the inflow angle.

8. REFERENCES.

1. Safety Analysis Team, Report No. SAT-01.1, September 24, 1997.

2. Title 14 CFR Part 25.571, Damage tolerance and fatigue evaluation of structure.

3. Title 14 CFR Part 25.907, Propeller vibration.

4. Title 14 CFR Part 23.907, Propeller vibration.

5. Advisory Circular 20-66A, Vibration and Fatigue Evaluation of Airplane Propellers.

6. Advisory Circular 35.37-1A, Guidance Material for Fatigue Limit Tests and Composite Blade Fatigue Substantiation.

7. Tipps, D.O., Skinn, D.A., Rustenburg, J.W., and Zeiler, T.A., "Statistical Loads Data for BE-1900D Aircraft in Commuter Operations," FAA report DOT/FAA/AR-00/11, April 2000.

8. Rustenburg, J.W., Skinn, D.A., and Tipps, D.O., "An Evaluation of Methods to Separate Maneuver and Gust Load Factors From Measured Acceleration Time Histories," FAA report DOT/FAA/AR-99/14, April 1999.

9. FAA Type Certificate Data Sheet, Number P-10NE, Revision 17, 4 September 2007.

10. Harlament, W.B. and Edinger, R., "Development of an Aircraft Composite Propeller," SAE Paper 790579, *Society of Automotive Engineers, Business Aircraft Meeting and Exposition*, Wichita, KS, 3-6 April 1979.

11. Law, A.M. and Kelton, W.D., *Simulation Modeling and Analysis*, McGraw Hill Higher Education, 3rd Edition, Chap. 6, April 2000.

12. Anonymous, *Jane's All the World's Aircraft 2004-2005*, Franklin Watts, New York, 2004.

13. FAA Type Certificate Data Sheet, Number A24CE, Revision 96, pp. 36-41, 20 November 2007.

APPENDIX A—CALCULATION OF UPWASH ANGLE

The Biot-Savart law is an electromagnetic equation that relates the intensity of a magnetic field near a current-carrying conductor to the magnitude of the current. When this law is applied to aerodynamics, current is equivalent to the vortex strength, and the magnetic field strength equivalent to the induced flow velocity. This law can be used to estimate the induced flow velocity in the neighborhood of a vortex filament. The Biot-Savart law is given in equation A-1, where the lengths and angles are defined in figure A-1.

$$dv = \frac{\Gamma}{4\pi r^2}\sin(\eta)\,ds \tag{A-1}$$

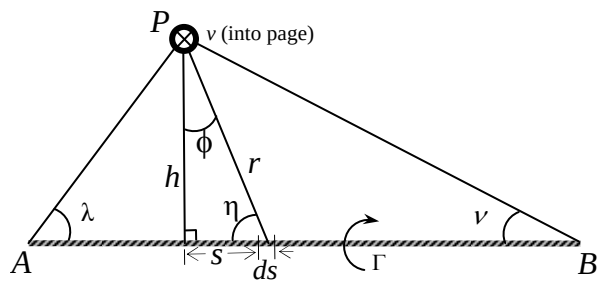

Figure A-1. Velocity (*V*) Induced at Point (*P*) by a Vortex of Strength (Γ) and Length (*AB*)

To find the total velocity induced by the vortex filament at point *P*, equation A-1 has to be integrated over the length of the vortex filament. From figure A-1, the relations given in equations A-2 through A-5, which are needed for integrating equation A-1, can be established.

$$\sin\eta = \cos\phi \tag{A-2}$$

$$s = h\tan\phi \tag{A-3}$$

$$r^2 = h^2\sec^2\phi \tag{A-4}$$

$$ds = h\sec^2\phi\, d\phi \tag{A-5}$$

Substituting these relations into equation A-1, the differential-induced velocity can be expressed in terms of a single variable, ϕ.

$$dv = \frac{\Gamma}{4\pi h}\cos(\phi)\,d\phi \tag{A-6}$$

The limits of the integration of equation A-6 are from point *A* to point *B* in figure A-1, which are given in terms of the angle ϕ in equations A-7 and A-8.

$$\phi_A = -\left(\frac{\pi}{2} - \lambda\right) \tag{A-7}$$

$$\phi_B = \left(\frac{\pi}{2} - \nu\right) \tag{A-8}$$

The result of the integration is given in equation A-9.

$$v = \frac{\Gamma}{4\pi h}\left(\cos\lambda + \cos\nu\right) \tag{A-9}$$

When this equation is applied to a semi-infinite vortex, the angle of the infinite end goes to zero, which then results in equation A-10.

$$v = \frac{\Gamma}{4\pi h}\left(\cos\lambda + 1\right) \tag{A-10}$$